Zebrafish as a model to study PERK function in developmental diseases: implications for Wolcott-Rallison syndrome

Liliana M. Almeida[a,b], Leonor Pereira Lima [a,b], Nuno A. S. Oliveira [a,b], Rui F. O. Silva [a,b], Bruno Sousa [a,b], José Bessa [c,d], Brígida R. Pinho [a,b], Jorge M. A. Oliveira [a,b]

[a]UCIBIO, Applied Molecular Biosciences Unit, Mitochondria and Neurobiology Lab, Faculty of Pharmacy, University of Porto, 4050-313 Porto, Portugal

[b]i4HB, Institute for Health and Bioeconomy, Department of Drug Sciences, Faculty of Pharmacy, University of Porto, 4050-313 Porto, Portugal

[c]IBMC, Instituto de Biologia Molecular e Celular, Universidade do Porto, 4200-135 Porto, Portugal

[d]i3S, Instituto de Investigação e Inovação em Saúde, Universidade do Porto, 4200-135 Porto, Portugal

Corresponding author:
Jorge M. A. Oliveira (jorgemao@ff.up.pt)
Departamento de Ciências do Medicamento, Laboratório de Farmacologia, Faculdade de Farmácia, Universidade do Porto
Rua de Jorge Viterbo Ferreira, 228, 4050-313 Porto, Portugal | Tel. +351 220428610

Abbreviations:
2-NBDglucose, (2-(7-Nitro-2,1,3-benzoxadiazol-4-yl)-D-glucosamine); ATF4, Activating Transcription Factor 4; CHOP, C/EBP homologous protein; dpf, days post-fertilization; dTC, d-tubocurarine; eIF2α, eukaryotic translation initiation factor 2α; ER, Endoplasmic reticulum; hfp, hours post-fertilization; GSK, GSK2606414; ISR, Integrated Stress Response; NPH, Nikon-Prior-Hamamatsu; PERK, Protein kinase R-like ER kinase; WRS, Wolcott-Rallison Syndrome

Complete text character count with spaces: 61 428.

Acknowledgments: Fundação para a Ciência e a Tecnologia (FCT): UIDB/04378/2020; UIDP/04378/2020; LA/P/0140/2020; SFRH/BD/138451/2018; DL57/2016/CP1346/CT0016; PTDC/BIA-MOL/3834/2021; CEECIND/03482/2018.

Running Title: Zebrafish PERK in developmental diseases

Abstract

Developmental diseases are challenging to investigate due to their clinical heterogeneity and relatively low prevalence. The Wolcott-Rallison Syndrome (WRS) is a rare developmental disease characterized by skeletal dysplasia and permanent neonatal diabetes due to loss-of-function mutations in the endoplasmic reticulum stress kinase PERK (EIF2AK3). The lack of efficient and less invasive therapies for WRS highlights the need for new animal models that replicate the complex pathological phenotypes, while preserving scalability for drug screening. Zebrafish exhibits high fecundity and rapid development that facilitate efficient and scalable *in vivo* drug testing. Here, we aimed to assess the potential of zebrafish to study PERK function and its pharmacological modulation, and as model organism of developmental diseases such as the WRS. Using bioinformatic analyses, we showed high similarity between human and zebrafish PERK. We used the pharmacological PERK inhibitor GSK2606414, which was bioactive in zebrafish, to modulate PERK function. Using transgenic zebrafish expressing fluorescent pancreatic markers and a fluorescent glucose probe, we observed that PERK inhibition decreased β cell mass and disrupted glucose homeostasis. By combining behavioural and functional assays, we show that PERK-inhibited zebrafish present marked skeletal defects and defective growth, as well as neuromuscular and cardiac deficiencies, which are clinically relevant in WRS patients, while sparing parameters like otolith area and eye/body ratio which are not associated with WRS. These results show that zebrafish holds potential to study PERK function and its pharmacological modulation in developmental disorders like WRS, assisting research on their pathophysiology and experimental treatments.

Keywords: developmental diseases; metabolic diseases; model organism; zebrafish; PERK; Wolcott-Rallison syndrome

62 **1. Introduction**

63

64 Protein kinase RNA-like endoplasmic reticulum kinase (PERK) is an endoplasmic reticulum
65 (ER) membrane kinase that activates in response to disruptions in ER protein homeostasis
66 (proteostasis) by promoting a protective response, the integrated stress response (ISR). Upon
67 activation by stress, PERK phosphorylates eukaryotic translation initiation factor 2α or (eIF2
68 α) that decreases global protein synthesis and thus alleviates the proteostasis system [1].
69 Additionally, ISR promotion by PERK boosts the synthesis of specific transcription factors
70 such as activating transcription factor 4 (ATF4) and C/EBP homologous protein (CHOP) that
71 regulate the expression of chaperones, proteases and components of the autophagic pathway,
72 thus contributing to proteostasis recovery [1]. During development, protein synthesis plays a
73 critical role in cell division, differentiation, and the rapid growth of embryos [2], and PERK is
74 essential for detecting protein misfolding and adjusting protein synthesis to maintain
75 proteostasis [3].

76 Global knockout of PERK in mice induces several developmental defects, namely
77 reduced bone density, mineralization and body size [4], loss of insulin-producing beta cells and
78 hyperglycaemia [5-7]. Additionally, PERK inhibition reduces skeletal muscle mass, and
79 strength [8] and impairs cardiac valve formation [9]. In humans, loss-of-function mutations in
80 the *EIF2AK3* gene encoding for PERK cause a rare (ORPHA:1667) autosomal recessive
81 developmental disease named Wolcott-Rallison Syndrome (WRS) [10].

82 Clinically, WRS is characterized by the presence of skeletal dysplasia and neonatal
83 diabetes mellitus [5]. Additionally, WRS patients may present broad spectrum symptoms –
84 such as motor neuropathy, intellectual deficit, early neurodegeneration, and cardiac
85 malformations – likely due to the widespread distribution of PERK with several loss-of-
86 function mutations totally or partially abolishing its kinase activity [11, 12]. The prognosis of

87 WRS patients is usually poor and death occurs at a young age (< 35 years old) from multiple
88 organ failure with predominant liver and renal dysfunction, and encephalopathy [5]. Existing
89 therapies include blood glucose control with insulin pumping and transplant of liver/pancreas
90 and kidney [13]. The scarcity of non-invasive and more effective therapeutic options for WRS
91 patients highlights the need for further therapeutic investigation, which requires efficient WRS
92 models.

93 The currently available *in vivo* models for developmental diseases such as WRS are
94 rodents with loss-of-function mutations in PERK that exhibit the WRS hallmarks – neonatal
95 diabetes and skeletal dysplasia [6, 7] – and the broad-spectrum phenotypes – cardiac, muscle
96 and cognitive abnormalities [8, 9, 14]. However, for exploratory studies of new therapeutics
97 that typically occur in large scales, there are efficiency advantages in using small vertebrates
98 such as zebrafish before testing the most promising candidates in rodent models. The small
99 vertebrate zebrafish is increasingly used to develop disease models given its advantageous
100 features: high fecundity, external fertilization, and rapid formation of complete organs, making
101 zebrafish ideal for investigating developmental diseases and for rapid and scalable *in vivo* drug
102 testing [15, 16]. Previous studies that targeted PERK in zebrafish, used either genetic
103 (morpholino knockdown) or pharmacological inhibition [17-19]. In such studies, PERK
104 inhibition with GSK2606414 was used in zebrafish adults to study sleep regulation [18], and
105 PERK inhibition with GSK2656157 or PERK knockdown was used to study redox regulation
106 and neurogenesis in zebrafish embryos [17, 19]. Thus, to the best of our knowledge, there are
107 no previous studies in zebrafish with a primary focus on studying PERK function in
108 developmental diseases, including WRS.

109 In the present study, we combined bioinformatic analyses, molecular biology techniques,
110 behaviour, and functional assays to assess the effects of pharmacological PERK inhibition in
111 zebrafish. We used transgenic zebrafish expressing pancreatic reporters and a fluorescent

112 glucose probe to assess diabetic-like phenotypes. We used functional and structural microscopy
113 to assess skeletal, neuromuscular, and cardiac phenotypes. Our data show that zebrafish holds
114 potential as a model to study PERK function in developmental disorders, such as WRS.
115

116 ## 2. Material and Methods

117

118 ### 2.1 Drugs, solvents, and solutions

119

120 GSK2606414 (Merck Millipore, 516535) was used to inhibit PERK [20] in zebrafish, as
121 previously done [18]. Stock drug solutions were prepared in anhydrous DMSO (Sigma,
122 276855). D-tubocurarine (dTC, Sigma, t2379) solution was prepared in MilliQ water and used
123 as a muscle relaxant. Prior to assays, stocks were diluted in embryo (E3) medium: 5 mM NaCl
124 (Sigma, S9888), 0.17 mM KCl (Chem-Lab, cl00.1133.1000), 0.33 mM CaCl2•2H2O (Panreac,
125 131232.1211), 0.33 mM MgCl2•6H2O (Sigma, TA523733) and 0.0001% methylene blue
126 (Sigma, M9140) [21]. Tricaine methanesulfonate (Sigma, E10521) was used as anesthetic at
127 0.02%. In the assay solutions, DMSO was always kept under 0.2% [22].

128

129 ### 2.2 Zebrafish maintenance and husbandry

130

131 Adult AB strain zebrafish were supplied by the Interdisciplinary Centre of Marine and
132 Environmental Research (CIIMAR, Portugal) and maintained in 45 L tanks at 28 ± 1°C on a
133 14 h:10 h light:dark cycle and handled for egg production as we previously detailed [23, 24].
134 Handling of zebrafish followed the European Directive 2010/63/EU and the Portuguese Law
135 (Decreto-Lei 113/2013). Briefly, adults (1:1, male:female) were placed in a 0.7 L breeding tank
136 with circulating water in contact with the main tank on the day before egg collection. Ninety
137 minutes after starting the light period, eggs were collected and washed. This time point was
138 recorded as 0 h post fertilization (hpf).

139

140 **2.3 Drug treatments**

141

142 Zebrafish were randomly distributed in 24-well plates (5 zebrafish/well; 0.5 mL E3/well) and
143 kept at 28 ± 1°C on a 14 h:10 h light: dark cycle throughout the assay. Zebrafish were
144 continuously exposed to GSK2606414 or solvent (DMSO) from 4 to 76 hpf and solutions were
145 renewed daily [23]. In each experiment, all drug concentrations were assayed at least in
146 duplicate wells (5 + 5 zebrafish). Experiments were repeated at least three times independently
147 (≥ 30 zebrafish) [25]. Tubocurarine (dTC) was incubated for 10 minutes before assays endpoint
148 in 5 zebrafish, in at least three independent experiments (≥ 15 zebrafish).

149

150 **2.4 Brightfield microscopy**

151

152 For brightfield microscopy, a stereomicroscope (Stemi DV4, Zeiss, Göttinger, Germany) or an
153 inverted microscope (Eclipse TE300, Nikon, Tokyo, Japan) were used. The inverted
154 microscope was attached to a motorized stage (ProScan, Prior) and a CCD camera (ORCA-
155 ER, Hamamatsu), all controlled by the open-source software Micro-Manager (v. 2.0;
156 https://micro-manager.org). This Nikon-Prior-Hamamatsu (NPH) imaging system was used to
157 perform the following brightfield imaging protocols:

158 ***2.4.1 Monitoring zebrafish development***

159 At regular time points (28, 52 and 76 hpf) zebrafish were scored as normal, abnormal,
160 or dead; hatched (ruptured chorion and free tail movement) or unhatched. Zebrafish
161 were classified as dead if lacking one of the following: somite formation, tail
162 detachment or heartbeat; as according to OECD guideline 236 [26]. Normal
163 development was as previously described [27]. Abnormalities were scored as cardiac
164 and skeletal (further into scoliosis, curly-up tail, or kyphosis). Dead zebrafish were

removed from the experiments and only live zebrafish were used in the following assays.

2.4.2 Morphometric analysis

Brightfield images were used for morphometric analysis of head-tail angle and body length of zebrafish. Body length was measured from the tip of the zebrafish head (between the eyes) to the end of the tail [28]. Trunk-tail angle was measured with the angle tool of ImageJ at the intersection between the rostral (trunk) and caudal (tail) notochord at the level of the anus (Figure 3 B). Both parameters (length and angle) were quantified by a researcher blinded to experimental conditions.

2.4.3 Heartbeat and atrio-ventricular coordination

Heartbeats were counted by microscopic visualization of at least two zebrafish per well (4 zebrafish per condition, per experiment), during 20 s, at 72-80 hpf [25]. Recordings of atrio-ventricular coordination were obtained by imaging live zebrafish for 90 seconds at 12 frames per second. After the experiments, the atrium and ventricle were visually identified, and the recordings were obtained with “Plot Z-axis profile” on ImageJ.

2.4.4 Tail coilings

Zebrafish spontaneous activity was assessed by monitoring tail coiling movements at 28 hpf in glass bottom 96-well plates. Each zebrafish was imaged for 3 minutes at a frequency of 4.5 frames per second and 2x2 or 4x4 binning [21]. After imaging, tail coilings were assessed by researchers blinded to experimental conditions.

2.4.5 Birefringence analysis

For muscle birefringence analysis, 76 hpf zebrafish were anesthetized immobilized on a glass surface, oriented laterally, and illuminated with linearly polarized light (Screen-Tech, ST-38). An orthogonal polarization filter was placed after the samples to block directly transmitted light. Thus, only light whose polarization angle is affected by the

190 sample is collected by the NPH microscope [29]. Pixel intensity in the trunk region was
191 measured by selecting the region of interest with ImageJ software by a researcher
192 blinded to experimental conditions.
193
194 **2.5 Touch-evoked escape response**
195
196 At 76 hpf, at least two zebrafish per well (6 zebrafish per condition) were submitted to 10
197 alternate touches to the head and to the tail with 10 µL pipette tip with a recovery time of 30
198 seconds [30]. Data are presented as response rates in percentage of total touches.
199
200 **2.6 Fluorescent labelling and microscopy of zebrafish**
201
202 At 73 hpf, zebrafish were incubated with a fluorescent glucose analogue - 600 µM 2-
203 NBDglucose (2-(7-Nitro-2,1,3-benzoxadiazol-4-yl)-D-glucosamine) (200 µL, Tebu-Bio,10-
204 1459) [31, 32]; and a positive control for neuromast labelling - Mitotracker Deep Red (1 µM,
205 Invitrogen, M22426) for 3 hours in 96 well plates (4 zebrafish /well). At 76 hpf, each zebrafish
206 was washed twice with E3 solution, anesthetized with 0.02% tricaine methanesulfonate
207 (Sigma, E10521) and imaged in a glass-bottom chamber. For imaging, we used the NPH
208 microscope with a monochromator (Polychrome II, Photonics). 2-NBDglucose was excited at
209 475 nm and Mitotracker Deep Red at 650 nm for 1 second. Emissions were collected using
210 band pass filters (Chroma 69008 – ET – ECFP/EYFP/mCherry) with a 10 × objective. Images
211 of the entire fish were stitched with the GNU image manipulation program (The GIMP
212 Development Team, 2019; https://www.gimp.org), before evaluation of anterior and posterior
213 neuromasts [33] by a researcher blinded to the treatment conditions.
214

215 **2.7 Imaging of fluorescent transgenic zebrafish**

216

217 Double transgenic zebrafish expressing GFP in insulin-producing β cells (endocrine pancreas)
218 and mCherry in somatostatin producing δ cells (endocrine pancreas), Tg(*ins:GFP,*
219 *sst:mCherry*), or expressing GFP in β cells and mCherry in elastase producing-cells (exocrine
220 pancreas), Tg(*ins:GFP, ela:mCherry*) [34], were obtained from José Bessa's laboratory at the
221 Institute for Research and Innovation in Health (i3s, University of Porto, Portugal). Transgenic
222 zebrafish were kept in 24-well plates (5 zebrafish/plate) with E3 media until the start of drug
223 treatments (DMSO 0.15%, GSK2606414 3–10 μM). We used two pharmacological
224 approaches: 1) GSK2606414 exposure from 4 hpf (before the principal islet of Langerhans is
225 formed within the endocrine pancreas) to 28, 76 or 148 hpf; 2) GSK2606414 exposure from
226 76 hpf (when the principal islet is already formed) to 148 hpf [35]. Drug solutions were
227 renewed daily. At the final time point (28, 76 or 148 hpf) zebrafish were anesthetized by rapid
228 cooling on ice and fixed in 4% paraformaldehyde overnight. Zebrafish were imaged with the
229 NPH inverted microscope. GFP was excited at 488 nm and mCherry was excited at 575 nm.
230 Emissions were collected using band pass filters (Chroma 59022 – EGFP/mCherry) with a 20
231 × objective. The area of GFP- or mCherry-labelled pancreas in each image was assessed with
232 the ImageJ software (https://imagej.nih.gov/ij) by a researcher blinded to the treatment
233 conditions.

234

235 **2.8 Western blot**

236

237 A pool of 24 to 27 zebrafish larvae were used per condition. Larvae were rinsed with ice-cold
238 system water twice before being placed in RIPA buffer (50 mM Tris (NZYTech, MB01601),
239 150 mM NaCl (Merck, S9888), 1 mM EDTA (Sigma-Aldrich, E6758), 1% IGEPAL CA-630

240 (Sigma-Aldrich, I3021), 1% sodium deoxycholate (Sigma-Aldrich, D6750), 0.1% sodium
241 dodecyl sulfate (Sigma-Aldrich, L3771) supplemented with a protease and phosphatase
242 inhibitor cocktail (Thermo Scientific, 78440). After 3 freeze-thaw cycles, samples were
243 homogenized with Precellys Evolution (6800 rpm, 5 × 42 s with 37 s interval) and centrifuged
244 at 12,000 × g (10 min, 4 °C). Supernatant protein concentrations were quantified by the
245 Bradford method. Protein extracts supplemented with Bolt LDS sample buffer (Invitrogen,
246 B0007) and Bolt sample reducing agent (Invitrogen, B0009) were denatured at 95 ºC for 5 min.
247 30 to 40 µg of protein were loaded into 4–15% Mini-PROTEAN® TGX™ Precast Protein Gels
248 (Biorad, 4561084), electrophoresed between 125 and 200 V for 30 min and wet-transferred to
249 PVDF membranes (Millipore, IPVH00010) overnight (30 V, 4ºC). Membranes were then
250 blocked (1 h, room temperature or overnight at 4ºC) with 5% bovine serum albumin (BSA,
251 NZYTech, MB04602) in PBS with 0.05% Tween 20 (PBST) and then incubated with primary
252 antibodies: anti-ATF4 (1:500, overnight, Proteintech Cat# 10835-1-AP, RRID: AB_2058600);
253 anti-CHOP (1:1000, overnight, Proteintech Cat# 15204-1-AP, RRID:AB_2292610); anti-
254 eIF2α (1:1000, overnight, Thermo Fisher Scientific Cat# AHO0802, RRID: AB_2536316);
255 anti-p-eIF2α (1:500, overnight, Thermo Fisher Scientific Cat# MA5-15133,
256 RRID:AB_10983400). After washing with PBST for 15 min, membranes were incubated with
257 respective horseradish peroxidase-conjugated secondary antibodies for 1 h: anti-mouse
258 (1:4000, 1 h, Thermo Fisher Scientific Cat# G-21040, RRID: AB_2536527); anti-rabbit
259 (1:4000, 1 h, Thermo Fisher Scientific Cat# G-21234, RRID:AB_2536530). Detection was
260 performed using a Chemiluminescent kit (Novex ECL, Invitrogen, WP20005) and a ChemiDoc
261 MP Imaging system (Bio-Rad). Membrane Coomassie (Sigma-Aldrich, 27816) staining was
262 used for loading control rather than proteins usually described as 'housekeeping', because the
263 levels of these proteins may change in certain biological or pathological conditions, while
264 coomassie stains all proteins with loading higher than 50 ng [36]. Densitometric analyses were

265 performed with the Image J software. In each independent experiment, samples from control
266 (0 µM GSK) and 10 µM GSK- treated zebrafish were run in the same gel.
267
268 **2.9 Bioinformatic analyses**
269 **2.9.1 Comparison of PERK orthologues**
270 Protein sequence data from zebrafish (*Danio rerio,* XP_005156642.2), human (*Homo*
271 *sapiens,* AAI26357.1), mouse (*Mus musculus,* AAH54809.1), fruit fly (*Drosophila*
272 *melanogaster,* AAF61200.1), and nematode (*Caenorhabditis elegans*, AAF61201.1)
273 were obtained from NCBI Protein (https://www.ncbi.nlm.nih.gov/protein/). The amino
274 acid sequence from the total human PERK protein and from its catalytic domain were
275 compared with its orthologue proteins from zebrafish, mouse, fruit fly, and nematode,
276 using the Protein BLAST tool (https://blast.ncbi.nlm.nih.gov/Blast.cgi). Additionally,
277 we determined the identity of the vital amino acids for GSK2606414 binding to the
278 catalytic site of PERK, by aligning the protein sequence from zebrafish and human.
279
280 **2.9.2 Zebrafish PERK 3D structure and molecular docking**
281 The predicted three-dimensional protein structures of zebrafish PERK (UniProt:
282 B8JI14) and human PERK (UniProt: Q9NZJ5) were obtained from AlphaFold Protein
283 Structure Database [37, 38]. To visualize and align the three-dimensional structures of
284 human PERK (PDB: 4g31), zebrafish PERK (UniProt: B8JI14), and GSK2606414, we
285 used UCSF ChimeraX [39]. The human GSK2606414-bound PERK structure (PDB:
286 4g31) was used as a starting model and superimposition with zebrafish PERK was done
287 in UCSF ChimeraX, using the Matchmaker tool. To assess the structural similarity
288 between zebrafish and human PERK and infer about GSK2606414 binding efficiency,

289 we calculated the root-mean-square deviation (RMSD) in ChimeraX software for the
290 total protein and for the catalytic site of zebrafish PERK.
291
292 **2.10 Statistical Analyses**
293
294 Data are shown as mean ± standard error of the mean (SEM) of the *n* specified in figure legends.
295 For experiments with only two groups, comparisons were made with the Student's *t*-test. For
296 single-factor (drug concentration) comparisons of multiple groups to their respective control,
297 we used One-Way ANOVA with Dunnett's *post-hoc* test. For two-factor (drug concentration
298 vs. time) analysis, we used Two-way ANOVA with Sidak's *post-hoc* test. For survival analysis
299 we used the Mantel-Cox (Log-rank) test. For all analyses, a *P* value under 0.05 was taken as
300 statistically significant. Data analyses were performed with Prism 6.0 (GraphPad).
301

302 **3. Results**

303

304 **3.1 The PERK-GSK2606414 binding site is conserved in humans and zebrafish**

305

306 To assess the potential of zebrafish to study PERK function and its pharmacological
307 modulation, we performed bioinformatic comparisons of the amino acid and structural identity
308 of zebrafish and human PERK, including specifically the binding site for the PERK inhibitor
309 GSK2606414. We selected GSK2606414 (hereafter GSK; not to be confused with glycogen
310 synthase kinase) because: it is one of the most used PERK inhibitors [1]; it was previously used
311 in zebrafish [18]; and the vital amino acids for its binding to PERK are identified [40, 41].

312 Although the zebrafish PERK homologue presented a 52-58% global amino acid
313 identity with human PERK, when comparing the 3D protein structure and the vital amino acids
314 for GSK binding in the catalytic site we observed a high similarity (Figure 1). Using molecular
315 visualization with ChimeraX, we observed that the average distance between the 3D structures
316 of zebrafish and human PERK is under 1 Å (Figure 1 C, D), indicating high similarity [42].
317 Moreover, using Protein BLAST, we observed that out of the 12 vital amino acids for GSK
318 binding to PERK [40, 41], there is only one difference between human and zebrafish (Figure 1
319 B). Such difference is a valine in human vs. isoleucine in zebrafish, and both amino acids are
320 hydrophobic.

321 Together, these results predict a high probability of GSK binding and inhibiting
322 zebrafish PERK. To test such prediction, we proceeded with functional assays.

323

324 **3.2 The PERK inhibitor GSK2606414 is bioactive in zebrafish**

325

326 To evaluate the effects of PERK inhibition in zebrafish, we evaluated the survival and hatching
327 of fish treated with increasing concentrations of GSK over time (Figure 2 A). We observed a
328 time-dependent decrease in survival, with 10 μM GSK being the lowest concentration that
329 induces a significant effect (50%) at 76 hpf (Figure 2 B). Zebrafish that failed to survive GSK
330 inside the chorion were excluded from hatching analysis. For surviving zebrafish, there was a
331 time-dependent increase in hatching without significant differences across GSK concentrations
332 (Figure 2 C). Next, we assessed the effect of GSK on the levels of PERK pathway (ISR)
333 biomarkers in the zebrafish at 76 hpf using western blot (Figure 2 D *i*). Results show that
334 treatment with GSK (10 μM, 72h) significantly decreased levels of phosphorylated of eIF2α,
335 ATF4, and CHOP (Figure 2 D *ii*-*vi*). Together, GSK effects confirm its bioactivity and are
336 compatible with PERK pathway inhibition as previously reported [18].
337
338 **3.3 PERK inhibition induces skeletal defects in zebrafish**
339 PERK inhibition in humans impairs skeletal development as evidenced by the presence of
340 skeletal dysplasia in WRS patients [5]. To assess the potential of zebrafish for studying the role
341 of PERK in zebrafish skeletal development, we exposed zebrafish embryos to the PERK
342 inhibitor from 4 to 76 hpf and monitored their development over time. GSK (10 μM) evoked a
343 significant time-dependent increase in morphological defects (Figure 3 A *i*). The most common
344 defect was a curly-up tail and a few cases of scoliosis (Figures 3 A *ii* - *iv*). Exposure to GSK
345 (10 μM) caused 20 ± 5 degrees change in the zebrafish trunk-tail angle at 76 hpf (Figure 3 B)
346 and a significant decrease in body length (Figure 3 C).
347 To ascertain if the morphological defects evoked by GSK are primarily skeletal or
348 involve an abnormal muscle contraction, we tested if the defects could be reversed by a muscle
349 relaxant (d-tubocurarine; dTC; antagonist of muscular nicotinic receptors [43]; effective in
350 zebrafish [44]). We confirmed dTC efficacy by observing a concentration-dependent decrease

351 in escape responses, with a maximal effect at 3 mM (Figure 3 D *i,ii*), as previously described
352 [44]. Even with the fully relaxing 3 mM dTC concentration there was no recovery of trunk-tail
353 angle in GSK-treated zebrafish (Figure 3 E). These results indicate that abnormal skeletal
354 development, rather than muscle contraction, is the main cause of the morphological defects.
355 To evaluate the selective toxicity of GSK, we examined otolith area (Supplementary
356 figure 1 A) and eye/body ratio (Supplementary figure 1 B) and found no significant effects in
357 such parameters that are unrelated to cardinal WRS phenotypes.
358 Collectively, these results indicate that upon PERK inhibition, zebrafish presented
359 skeletal abnormalities and growth retardation, indicating that the small vertebrate holds
360 potential to study the role of PERK in skeletal development.
361
362 **3.4 PERK inhibition delays endocrine pancreas development and limits glucose uptake**
363 **in zebrafish**
364
365 PERK is involved in blood glucose control by governing insulin production and β-cell mass.
366 In WRS patients, lack of PERK leads to decreased β-cell mass, impaired insulin production
367 and neonatal diabetes [45, 46]. Exocrine pancreas dysfunction associated with loss of PERK in
368 acinar cells may occur, although with a prevalence of 10.6% of WRS patients [47, 48]. Thus,
369 we explored if zebrafish could be used as an animal model to study PERK's role in pancreatic
370 development, ascertaining the effects of PERK inhibition in exocrine and endocrine pancreas
371 development.
372 We used two transgenic zebrafish lines expressing GFP in insulin-producing β-cells
373 (Figure 4 A). One line also expressed mCherry in somatostatin-producing δ-cells from the
374 endocrine pancreas – Tg(*ins:GFP, sst:mCherry*). The other line expressed mCherry in elastase-

375 producing exocrine pancreas –Tg(*ins:GFP, ela:mCherry*). We exposed both lines to GSK (10
376 μM) and measured the respective GFP/mCherry labelled areas as proxies for cell mass.
377 To test if the effects of GSK inhibition were selective for the early embryo
378 development, we used two exposure protocols: the *early exposure protocol* (Figure 4 B *i*)
379 started before the formation of the first Langerhans islet (endocrine pancreas); the *late exposure*
380 *protocol* started after islet formation (Figure 4 B *ii*). Early PERK inhibition (4 hpf) delayed
381 development of the endocrine pancreas, significantly decreasing β and δ cell mass at 28 hpf,
382 which seems to recover overtime (Figure 4 C *i*, D *i*). With late inhibition (76 hpf), we found no
383 significant differences in endocrine cell mass (Figure 4 C *ii*, D *ii*). Regarding the exocrine
384 pancreas mass, *ela:mCherry* fluorescence was only detectable at 148 hpf, and no significant
385 differences were found with either early or late GSK exposure protocols (Figure 4 E). These
386 findings support the hypothesis that PERK inhibition selectively delayed the early embryonic
387 development of the endocrine pancreas.
388 To test if delayed endocrine development affected glucose homeostasis, we measured
389 the uptake of a fluorescent glucose probe (2-NBDglucose [31]) in zebrafish treated with GSK
390 from 4 to 76 hpf (early exposure protocol). 2-NBDglucose uptake was measured in neuromast
391 cells, given their direct exposure to probes in the external media, using Mitotracker Deep Red
392 as a positive control for neuromast staining. We found that early PERK inhibition significantly
393 decreased the uptake of 2-NBDglucose (Figure 5 A, B). These results show that upon PERK
394 inhibition, zebrafish present a diabetic-like phenotype that resembles WRS with delayed
395 endocrine pancreas development and impaired glucose homeostasis, highlighting zebrafish as
396 a potential model to study the effects of PERK on pancreatic development.
397
398 **3.5 PERK inhibition evokes neuromuscular and cardiac impairments in zebrafish**
399

400 Beyond impairments in skeletal and pancreatic development, PERK inhibition also impairs the
401 development of cardiac valves and skeletal muscle, and can lead to neurodegeneration [5, 8,
402 9]. To test if zebrafish holds potential to study the mechanisms behind PERK effects on
403 neuromuscular development, we assessed spontaneous tail-coiling and touch-evoked escape
404 responses upon PERK inhibition [49-51]. We found that 10 μM GSK significantly increased
405 tail-coiling events in early development (28 hpf embryos inside the chorion; Figure 6 A) and
406 significantly decreased escape responses in later development (76 hpf larvae; Figure 6 B). To
407 test for altered muscle integrity, we assessed the arrangement of sarcomeres by measuring how
408 well they diffracted polarized light (birefringence assay) [52] (Figure 6 C *i*). Treatment with
409 10 μM GSK significantly decreased muscle birefringence intensity (Figure 6 C *ii, iii*). Next,
410 we monitored cardiac morphology and function in PERK-inhibited zebrafish [11, 53]. We
411 found that 10 μM GSK induced a time-dependent increase in pericardial oedema (Figure 7 A).
412 We monitored heart rate at 76 hpf and observed that 10 μM GSK induced bradycardia without
413 altering atrio-ventricular coordination (Figure 7 B).

414 These results are compatible with PERK-inhibited zebrafish presenting cardiac and
415 neuromuscular abnormalities in morphology and function, suggesting that zebrafish are
416 suitable animal models to study PERK effects on cardiac and neuromuscular development and
417 function.

418

419

420 **4. Discussion**

421 In the present study we expand the understanding of PERK's role in the embryonic
422 development of multiple zebrafish organs, adding to previous knowledge of PERK's function
423 in zebrafish sleep regulation and oxidative stress handling [17-19]. Specifically, we show that
424 PERK inhibited-zebrafish presented skeletal defects and diabetic-like phenotypes, cardiac and

425 neuromuscular alterations. These phenotypes resemble the clinical features of patients with
426 loss-of-function mutation in PERK, such as in the Wolcott-Rallison syndrome. Thus, these
427 results support the potential of zebrafish to study PERK's role in developmental diseases with
428 clinically relevant multisystem involvement such as the Wolcott-Rallison syndrome.
429
430 **4.1 Pharmacological inhibition of PERK**
431 To inhibit PERK activity in zebrafish we used a pharmacological approach with
432 GSK2606414 (GSK), one of the most used PERK inhibitors in the scientific literature [1].
433 PERK inhibition with GSK decreased ISR activation in animals such as mice [54], frogs [55]
434 and flies [18]. In the present study, we show that GSK decreases the levels of ISR markers in
435 zebrafish, which suggests that GSK is bioactive and effective in decreasing PERK pathway
436 activity. Additionally, GSK incubation produced robust results consistent with WRS-
437 associated phenotypes (skeletal impairments and diabetic-like phenotype), while sparing non-
438 WRS-associated parameters as otolith area and eye/body ratio, being compatible with selective
439 effects of PERK inhibition. We cannot rule out the possibility that GSK is also acting on off-
440 targets, such as kinases of the c-KIT and RIPK families [56, 57]. However, previous studies
441 that genetically inhibited KITa/b and RIPK3 activities in zebrafish did not show the structural
442 alterations and defective growth we observed with GSK-treatment [58, 59].
443
444 **4.2 Skeletal impairments**
445 Regarding the development of the skeleton, zebrafish and humans share great similarities
446 in anatomy and physiology including the main skeletal cell types and development pathways
447 [60]. Mechanistically, PERK's loss-of-function delays the differentiation and proliferation of
448 osteoblasts and decreases the secretion of type I collagen. As these are essential factors for
449 normal bone development, PERK's loss-of-function decreases bone mineralization [4]. Due to

450 PERK loss-of-function, WRS patients present short stature and skeletal dysplasia, particularly
451 noticeable in long bones, pelvis, and vertebrae [5]. Mice with PERK ablation exhibit postnatal
452 growth retardation, bone loss and skeletal dysplasia [7, 61]. Here, we show that zebrafish
453 treated with a PERK inhibitor also present decreased growth and skeletal defects.
454

455 **4.3 Diabetic-like phenotype**

456 PERK controls pancreatic development and insulin production since PERK ablation in mice
457 reduced β cell mass, impaired proinsulin maturation and induced hyperglycaemia [6, 62-64].
458 In humans, WRS neonatal diabetes is insulin requiring but not autoimmune, being caused by
459 loss of PERK function, which likely disrupts insulin maturation in the endoplasmic reticulum
460 [5-7]. WRS patients also present a hypoplastic pancreas, with smaller insulin-secreting β cells
461 [65]. In the present study, we show that early PERK inhibition with GSK2606414 in zebrafish
462 delays endocrine pancreas development, reducing β-cell mass. Although β-cell mass recovers
463 overtime, as assessed by the GFP reporter in transgenic zebrafish, insulin production likely
464 remains partly compromised given the reduced uptake of 2-NBDglucose. Recovery of β -cell
465 mass in zebrafish can be explained by its ability to regenerate pancreatic tissue [66, 67]. As
466 this recovery occurs in the presence of the PERK inhibitor, it likely involves PERK-
467 independent protective mechanisms. The identification of such mechanisms may assist the
468 development of novel WRS therapies that harness the potential of PERK-independent
469 pancreatic recovery.

470 In contrast to the delayed development of the zebrafish endocrine pancreas, we found no
471 effect of 10 μM GSK2606414 upon the mass of the exocrine pancreas at 148 hpf. While
472 different mechanisms regulate development of the endocrine and exocrine pancreas, we cannot
473 rule out that our zebrafish model may present differences in the mass of the exocrine pancreas
474 upon extended exposure to the PERK inhibitor. Additionally, exocrine pancreas alterations are

475 relatively uncommon occurring only in 10.6% of WRS patients [48]. Still, one hypothesis to
476 explain the differential effect of inhibiting PERK in endocrine and exocrine pancreas might
477 reside in PERK's cell autonomous effects. Selective PERK knockout in the endocrine pancreas
478 of mice induces hyperglycaemia and decreased β cell mass but does not induce exocrine
479 atrophy. Conversely, PERK knockout in the exocrine pancreas induces atrophy in the exocrine
480 portion but not in the endocrine portion and without causing diabetes [47, 63]. Future studies
481 using selective PERK knockout in zebrafish pancreatic cell sub-types may contribute to
482 understand differential pancreatic vulnerability.
483
484 **4.4 Neuromuscular and cardiac development**
485 In addition to skeletal and pancreatic development, PERK ablation also impairs the
486 development of skeletal muscle and heart valves [4, 9], which explains why WRS patients may
487 also present neuromuscular and cardiac dysfunctions [11, 53, 68]. Here, we show that zebrafish
488 developed neuromuscular and cardiac abnormalities upon PERK inhibition, as discussed
489 below.
490 Regarding neuromuscular function, WRS patients display brain structural abnormalities,
491 microcephaly, and muscle weakness, by mostly unknown mechanisms associated with the loss
492 of PERK function [5, 12]. We show that PERK inhibition increased spontaneous tail
493 movements in early zebrafish embryonic development, which arise in a spinal central pattern
494 generator that provides rhythmic depolarizations [49, 51]. Later in development, PERK
495 inhibition manifested as decreased touch-evoked escape response, which arise in sensory
496 neurons [50, 51]. Skeletal defects and impairments in muscle integrity might also contribute
497 to the decreased escape responses in zebrafish treated with GSK2606414. Interestingly,
498 selective PERK ablation in either skeletal muscle or nigral dopaminergic neurons sufficed to

499 evoke motor impairments in mice [8, 69]. Thus, the mechanisms causing motor impairment
500 upon PERK inhibition likely combine dysfunctions originating in neurons and in muscle.
501 Regarding cardiac alterations, clinicians reported multiple cases of WRS patients with
502 structural malformations and altered rhythmicity [53, 70], and PERK knockout mice show
503 abnormal heart valves [9]. The transparency of young zebrafish allows non-invasive
504 examination of heart structure and function. Furthermore, their small body size permits oxygen
505 diffusion, enabling the detection of developmental cardiac abnormalities that would be fatal in
506 mammals due to inadequate oxygen supply [71]. Our data demonstrate that inhibiting PERK
507 in zebrafish induces morphologic and functional cardiac abnormalities. Nonetheless, further
508 functional and structural measurements are necessary to characterize the cardiac abnormalities
509 and assess their relevance for broad-spectrum WRS.
510
511 **5. Conclusions**
512 In this study, we demonstrate the potential of the small vertebrate zebrafish for the study of
513 developmental diseases, namely diseases caused by PERK inhibition such as the WRS. We
514 show that pharmacological inhibition of PERK with GSK2606414 induced skeletal defects,
515 defective growth, and diabetic-like phenotypes, such as delayed development of the endocrine
516 pancreas and altered glucose homeostasis, which also occur in WRS patients. Inhibiting PERK
517 in zebrafish also produced neuromuscular and cardiac abnormalities, while sparing non-WRS
518 associated parameters such as otolith area and eye/body ratio. In future studies, CRISPR/Cas9
519 technology can be used to generate zebrafish models with conditional/selective expression of
520 human PERK with WRS-driving mutations [72]. Also, future research on the mechanisms
521 governing PERK-independent pancreatic regeneration in zebrafish may uncover potential
522 therapeutic avenues for diabetic patients. Lastly, the scalability of zebrafish models holds great

523 potential to enhance the efficiency of drug screening against developmental diseases like the

524 WRS.

Declarations

CRediT authorship contribution statement

Liliana M. Almeida: Conceptualization, Methodology, Investigation, Validation, Data curation, Visualization, Formal analysis, Writing – original draft, Writing – review and editing; **Leonor Pereira Lima:** Investigation, Validation, Formal analysis, Visualization, Writing – review and editing; **Nuno A. S. Oliveira:** Investigation, Methodology, Validation, Visualization, Formal analysis, Writing – review and editing; **Rui F. O. Silva:** Investigation, Validation, Formal analysis; **Bruno Sousa:** Investigation, Validation; **José Bessa:** Methodology, Resources, Writing – review and editing, Funding acquisition; **Brígida R. Pinho:** Conceptualization, Methodology, Writing – review and editing, Supervision; **Jorge M. A. Oliveira:** Conceptualization, Methodology, Resources, Writing – review and editing; Funding acquisition, Project administration, Supervision.

Funding

Work in JMAO's lab was supported by the FCT – Fundação para a Ciência e a Tecnologia, Portugal – (UIDB/04378/2020; UIDP/04378/2020; LA/P/0140/2020). LMA acknowledges FCT for PhD fellowship (SFRH/BD/138451/2018). BRP acknowledges FCT for funding through program DL57/2016 - Norma transitória (DL57/2016/CP1346/CT0016). JB's laboratory was supported by Fundação para a Ciência e a Tecnologia (FCT) in the framework of the project PTDC/BIA-MOL/3834/2021. JB was supported by a FCT contract (CEECIND/03482/2018).

Competing Interests

The authors have no relevant financial or non-financial interests to disclose.

550 **Figure legends**

551

552 **Figure 1.** Bioinformatic analyses of PERK identity and GSK2606414-binding in human vs
553 zebrafish. (**A**) Percentage of identity between human, nematode (*Caenorhabditis elegans*), fruit
554 fly (*Drosophila melanogaster*), zebrafish (*Danio rerio*) and mouse (*Mus musculus*) PERK
555 (total and catalytic domain); Protein BLAST. (**B**) Comparison of vital GSK2606414 (GSK)-
556 binding amino acids in the catalytic domain of human and zebrafish PERK. Valine 651 in
557 human (yellow) is substituted by the also hydrophobic Isoleucine (red) in zebrafish; Protein
558 BLAST. (**C**) Predicted GSK (purple, #) binding to human (light blue) and zebrafish (dark blue)
559 PERK; ChimeraX. (**D**) Root Mean Square Deviation (RMSD) for the comparison between
560 human and zebrafish PERK tertiary structures and respective reference values; ChimeraX.

561

562 **Figure 2.** GSK2606414 effects on zebrafish survival, hatching, and PERK pathway
563 biomarkers. (**A**) Experimental timeline. (**B**) Zebrafish survival when exposed to GSK2606414
564 (GSK; 0-10 μM) over time (4-76 hours post-fertilization; hpf); n = 50-234 zebrafish, 5
565 independent breedings, Mantel-Cox test for survival, $^{*}P < 0.05$ vs. 0 μM GSK (control). (**C**)
566 Hatching of zebrafish treated with GSK; n= 50-234 zebrafish, 5 breedings, Two-Way ANOVA,
567 time effect: $^{\#}P < 0.05$. (**D**) Western blot of protein samples from 76 hpf zebrafish that survived
568 GSK treatment: *i*) Schematic representation of the PERK pathway biomarkers; *ii-vi*)
569 Representative blots and quantifications; n = 4 independent experiments (pool of 24-27 larvae
570 per condition and per experiment; *t*-test: $^{*}P < 0.05$.

571

572 **Figure 3.** GSK2606414-induced skeletal abnormalities in zebrafish. (**A**) (*i*) Morphological
573 defects following GSK2606414 (GSK) (0-10 μM) treatment overtime; $^{*}P < 0.05$, 10 vs. 0 μM
574 GSK; $^{\#}P<0.05$, effect of time for 10 μM GSK, two-way ANOVA with Sidak *post-hoc*; n = 50-

575 234 zebrafish; 5 independent experiments. (*ii-v*) Proportion of curly-up tail and scoliosis at 76
576 hpf, and representative images. (**B, C**) Measurements (blue lines) and quantifications of trunk-
577 tail angle and body length at 76 hpf; *$P < 0.05$ vs 0 μM GSK, One-Way ANOVA with
578 Dunnett's *post-hoc*; $n = 15$ zebrafish, 3 independent experiments. (**D**) Effect of muscle relaxant
579 d-tubocurarine (dTC, 0.03–3 mM) on escape responses after head or tail touch at 76 hpf; Grey
580 bands are mean ± SEM for control zebrafish; *$P < 0.05$ vs 0 mM dTC, One-Way ANOVA with
581 Dunnett's *post-hoc, n* = 15 zebrafish, 3 independent experiments. (**E**) (*i-iv*) Representative
582 images of zebrafish for the indicated-treatments. (*v*) Quantification of zebrafish with
583 morphological defects at 76 hpf for the indicated treatments. *$P < 0.05$ vs control, One-Way
584 ANOVA with Sidak's *post-hoc*, $n = 15$ zebrafish; 3 independent breedings. Blue arrows: curly-
585 up tail.
586
587 **Figure 4.** Pancreatic development in transgenic zebrafish. **(A)** Representative images of normal
588 pancreas development in Tg(*ins:GFP, sst:mCherry*) and Tg(*ins:GFP, ela:mCherry*) zebrafish.
589 (**B)** early (*i*) and late (*ii*) GSK2606414 (GSK)-exposure protocols. (**C-E**) Area measurements
590 for *ins:GFP* (green, insulin-producing *β*-cells), *sst:mCherry* (red, somatostatin-producing *δ*-
591 cells), and *ela:mCherry* (red, elastase-producing exocrine cells), in zebrafish exposed to 10 μM
592 GSK since 4 hpf (*i*, early exposure) or since 76 hpf (*ii*, late exposure). *$P < 0.05$, *t*-test, $n = 4$-
593 33 larvae. Representative images of GFP and mCherry are shown below respective bars.
594
595 **Figure 5.** GSK2606414 effects on 2-NBDglucose uptake in zebrafish. (**A**) Representative
596 brightfield and fluorescence images of zebrafish at 76 hpf, following treatment with (*i*) 0 μM
597 (control) or (*ii*) 10 μM GSK2606414 since 4 hpf. Images show the functional labelling at 76
598 hpf with the fluorescent glucose analogue 2-NBDglucose (2-NBDG; labels neuromasts that
599 upload glucose), and with the MitoTracker Deep Red probe (labels mitochondria in

600 neuromasts, working as positive control for neuromast presence). Circles in the "Merge"
601 images highlight either neuromasts containing 2-NBDglucose and MitoTracker (yellow
602 circles), or containing MitoTracker only (red circles). Below, 2x amplified images of the tails
603 are provided with arrowheads marking neuromasts from the zebrafish lateral line on the side
604 proximal to the microscope objective (the paired neuromasts from the lateral line on the other
605 side, distal to the objective, are without arrows). (**B**) Quantification of neuromasts labelled with
606 2-NBDglucose. *$P < 0.05$, t-test, n = 9-12 zebrafish per condition.
607
608 **Figure 6.** GSK2606414 effects on neuromotor responses and muscle integrity. (**A**) (*i*)
609 Representative tail coiling time-lapse: white line highlights notochord movement. (*ii*)
610 Quantification of tail coiling in 28 hpf zebrafish treated with GSK2606414 (GSK) since 4 hpf;
611 n = 23-26 zebrafish. (**B**) Quantification of escape responses after head (*i*) or tail (*ii*) touches at
612 76 hpf; n = 13-114 zebrafish. (**C**) (*i*) Schematic representation of the birefringence assay for
613 muscle integrity; (*ii*) Representative images of muscle birefringence at 76 hpf. (*iii*)
614 Quantification of birefringence intensity; n = 15 zebrafish. (**A-C**) Grey bands are mean ± SEM
615 for 0 μM GSK (control); *$P < 0.05$ vs. (control), One-Way ANOVA with Dunnett's *post-hoc*.
616
617 **Figure 7.** GSK2606414-induced morphological and functional cardiac defects. (**A**) (*i*)
618 Quantification of live zebrafish with pericardial oedema at the indicated hpf and GSK
619 concentrations. *$P < 0.05$, 10 vs. 0 μM GSK (control); two-way ANOVA with Sidak *post-hoc*
620 n= 50-234 zebrafish; 5 independent experiments. (*ii,iii*) Representative images of zebrafish
621 treated with GSK vs. control; blue arrow: pericardial oedema. (**B**) (*i*) Heartbeats per minute
622 (bpm) of 76 hpf zebrafish exposed to the indicated GSK concentrations since 4 hpf; Grey band
623 is mean ± SEM for control; *$P < 0.05$ vs control, One-Way ANOVA with Dunnett's *post-hoc*,

624 *n* = 13-116 zebrafish; (*ii*) Representative images of the heart and plots of atrio-ventricular

625 coordination in control and 10 μM GSK-treated zebrafish (a: atrium – red; v: ventricle – blue).

626

627 **References**

628

629 [1] L.M. Almeida, B.R. Pinho, M.R. Duchen, J.M.A. Oliveira, The PERKs of mitochondria
630 protection during stress: insights for PERK modulation in neurodegenerative and metabolic
631 diseases, Biol Rev Camb Philos Soc, (2022).

632 [2] L. Peshkin, M. Wuhr, E. Pearl, W. Haas, R.M. Freeman, Jr., J.C. Gerhart, A.M. Klein, M.
633 Horb, S.P. Gygi, M.W. Kirschner, On the Relationship of Protein and mRNA Dynamics in
634 Vertebrate Embryonic Development, Dev Cell, 35 (2015) 383-394.

635 [3] P. Wang, J. Li, J. Tao, B. Sha, The luminal domain of the ER stress sensor protein PERK
636 binds misfolded proteins and thereby triggers PERK oligomerization, J Biol Chem, 293 (2018)
637 4110-4121.

638 [4] J. Wei, X. Sheng, D. Feng, B. McGrath, D.R. Cavener, PERK is essential for neonatal
639 skeletal development to regulate osteoblast proliferation and differentiation, J Cell Physiol, 217
640 (2008) 693-707.

641 [5] C. Julier, M. Nicolino, Wolcott-Rallison syndrome, Orphanet J Rare Dis, 5 (2010) 29.

642 [6] H.P. Harding, H. Zeng, Y. Zhang, R. Jungries, P. Chung, H. Plesken, D.D. Sabatini, D.
643 Ron, Diabetes mellitus and exocrine pancreatic dysfunction in perk-/- mice reveals a role for
644 translational control in secretory cell survival, Mol Cell, 7 (2001) 1153-1163.

645 [7] P. Zhang, B. McGrath, S. Li, A. Frank, F. Zambito, J. Reinert, M. Gannon, K. Ma, K.
646 McNaughton, D.R. Cavener, The PERK eukaryotic initiation factor 2 alpha kinase is required
647 for the development of the skeletal system, postnatal growth, and the function and viability of
648 the pancreas, Mol Cell Biol, 22 (2002) 3864-3874.

649 [8] Y.S. Gallot, K.R. Bohnert, A.R. Straughn, G. Xiong, S.M. Hindi, A. Kumar, PERK
650 regulates skeletal muscle mass and contractile function in adult mice, FASEB J, 33 (2019)
651 1946-1962.

652 [9] T. Shimizu, K. Maruyama, T. Kawamura, Y. Urade, Y. Wada, PERK participates in cardiac
653 valve development via fatty acid oxidation and endocardial-mesenchymal transformation, Sci
654 Rep, 10 (2020) 20094.
655 [10] M. Delepine, M. Nicolino, T. Barrett, M. Golamaully, G.M. Lathrop, C. Julier, EIF2AK3,
656 encoding translation initiation factor 2-alpha kinase 3, is mutated in patients with Wolcott-
657 Rallison syndrome, Nat Genet, 25 (2000) 406-409.
658 [11] V. Senee, K.M. Vattem, M. Delepine, L.A. Rainbow, C. Haton, A. Lecoq, N.J. Shaw, J.J.
659 Robert, R. Rooman, C. Diatloff-Zito, J.L. Michaud, B. Bin-Abbas, D. Taha, B. Zabel, P.
660 Franceschini, A.K. Topaloglu, G.M. Lathrop, T.G. Barrett, M. Nicolino, R.C. Wek, C. Julier,
661 Wolcott-Rallison Syndrome: clinical, genetic, and functional study of EIF2AK3 mutations and
662 suggestion of genetic heterogeneity, Diabetes, 53 (2004) 1876-1883.
663 [12] J. Bruch, C. Kurz, A. Vasiljevic, M. Nicolino, T. Arzberger, G.U. Hoglinger, Early
664 Neurodegeneration in the Brain of a Child Without Functional PKR-like Endoplasmic
665 Reticulum Kinase, J Neuropathol Exp Neurol, 74 (2015) 850-857.
666 [13] A.G. Tzakis, M.J. Nunnelley, A. Tekin, L.D. Buccini, J. Garcia, K. Uchida, H.L. Neville,
667 M.A. Nares, P. Ruiz, O. Bodamer, Liver, pancreas and kidney transplantation for the treatment
668 of Wolcott-Rallison syndrome, Am J Transplant, 15 (2015) 565-567.
669 [14] M.A. Trinh, H. Kaphzan, R.C. Wek, P. Pierre, D.R. Cavener, E. Klann, Brain-specific
670 disruption of the eIF2alpha kinase PERK decreases ATF4 expression and impairs behavioral
671 flexibility, Cell Rep, 1 (2012) 676-688.
672 [15] T. Teame, Z. Zhang, C. Ran, H. Zhang, Y. Yang, Q. Ding, M. Xie, C. Gao, Y. Ye, M.
673 Duan, Z. Zhou, The use of zebrafish (Danio rerio) as biomedical models, Anim Front, 9 (2019)
674 68-77.
675 [16] T.Y. Choi, T.I. Choi, Y.R. Lee, S.K. Choe, C.H. Kim, Zebrafish as an animal model for
676 biomedical research, Exp Mol Med, 53 (2021) 310-317.

677 [17] K. Mukaigasa, T. Tsujita, V.T. Nguyen, L. Li, H. Yagi, Y. Fuse, Y. Nakajima-Takagi, K.
678 Kato, M. Yamamoto, M. Kobayashi, Nrf2 activation attenuates genetic endoplasmic reticulum
679 stress induced by a mutation in the phosphomannomutase 2 gene in zebrafish, Proc Natl Acad
680 Sci U S A, 115 (2018) 2758-2763.
681 [18] S. Ly, D.A. Lee, E. Strus, D.A. Prober, N. Naidoo, Evolutionarily Conserved Regulation
682 of Sleep by the Protein Translational Regulator PERK, Curr Biol, 30 (2020) 1639-1648 e1633.
683 [19] B. Jin, L. Xie, D. Zhan, L. Zhou, Z. Feng, J. He, J. Qin, C. Zhao, L. Luo, L. Li, Nrf2
684 dictates the neuronal survival and differentiation of embryonic zebrafish harboring
685 compromised alanyl-tRNA synthetase, Development, 149 (2022).
686 [20] S.R. Stockwell, G. Platt, S.E. Barrie, G. Zoumpoulidou, R.H. Te Poele, G.W. Aherne, S.C.
687 Wilson, P. Sheldrake, E. McDonald, M. Venet, C. Soudy, F. Elustondo, L. Rigoreau, J. Blagg,
688 P. Workman, M.D. Garrett, S. Mittnacht, Mechanism-based screen for G1/S checkpoint
689 activators identifies a selective activator of EIF2AK3/PERK signalling, PLoS One, 7 (2012)
690 e28568.
691 [21] N.A.S. Oliveira, B.R. Pinho, J. Pinto, P. Guedes de Pinho, J.M.A. Oliveira, Edaravone
692 counteracts redox and metabolic disruptions in an emerging zebrafish model of sporadic ALS,
693 Free Radic Biol Med, 217 (2024) 126-140.
694 [22] J. Hoyberghs, C. Bars, M. Ayuso, C. Van Ginneken, K. Foubert, S. Van Cruchten, DMSO
695 Concentrations up to 1% are Safe to be Used in the Zebrafish Embryo Developmental Toxicity
696 Assay, Front Toxicol, 3 (2021) 804033.
697 [23] R.F.O. Silva, B.R. Pinho, M.M. Santos, J.M.A. Oliveira, Disruptions of circadian rhythms,
698 sleep, and stress responses in zebrafish: New infrared-based activity monitoring assays for
699 toxicity assessment, Chemosphere, 305 (2022) 135449.

700 [24] B.R. Pinho, S.D. Reis, R.C. Hartley, M.P. Murphy, J.M.A. Oliveira, Mitochondrial
701 superoxide generation induces a parkinsonian phenotype in zebrafish and huntingtin
702 aggregation in human cells, Free Radic Biol Med, 130 (2019) 318-327.
703 [25] B.R. Pinho, M.M. Santos, A. Fonseca-Silva, P. Valentao, P.B. Andrade, J.M. Oliveira,
704 How mitochondrial dysfunction affects zebrafish development and cardiovascular function: an
705 in vivo model for testing mitochondria-targeted drugs, Br J Pharmacol, 169 (2013) 1072-1090.
706 [26] OECD, Test No. 236: Fish Embryo Acute Toxicity (FET) Test, (2013).
707 [27] C.B. Kimmel, W.W. Ballard, S.R. Kimmel, B. Ullmann, T.F. Schilling, Stages of
708 embryonic development of the zebrafish, Dev Dyn, 203 (1995) 253-310.
709 [28] R. Martinez, L. Navarro-Martin, C. Luccarelli, A.E. Codina, D. Raldua, C. Barata, R.
710 Tauler, B. Pina, Unravelling the mechanisms of PFOS toxicity by combining morphological
711 and transcriptomic analyses in zebrafish embryos, Sci Total Environ, 674 (2019) 462-471.
712 [29] N.A.S. Oliveira, B.R. Pinho, J.M.A. Oliveira, Swimming against ALS: How to model
713 disease in zebrafish for pathophysiological and behavioral studies, Neurosci Biobehav Rev,
714 148 (2023) 105138.
715 [30] B.R. Pinho, S.D. Reis, P. Guedes-Dias, A. Leitao-Rocha, C. Quintas, P. Valentao, P.B.
716 Andrade, M.M. Santos, J.M. Oliveira, Pharmacological modulation of HDAC1 and HDAC6 in
717 vivo in a zebrafish model: Therapeutic implications for Parkinson's disease, Pharmacol Res,
718 103 (2016) 328-339.
719 [31] J. Lee, D.W. Jung, W.H. Kim, J.I. Um, S.H. Yim, W.K. Oh, D.R. Williams, Development
720 of a highly visual, simple, and rapid test for the discovery of novel insulin mimetics in living
721 vertebrates, ACS Chem Biol, 8 (2013) 1803-1814.
722 [32] L. Wang, H. Kong, M. Jin, X. Li, R. Stoika, H. Lin, K. Liu, Synthesis of disaccharide
723 modified berberine derivatives and their anti-diabetic investigation in zebrafish using a
724 fluorescence-based technology, Org Biomol Chem, 18 (2020) 3563-3574.

725 [33] D. Stengel, F. Zindler, T. Braunbeck, An optimized method to assess ototoxic effects in
726 the lateral line of zebrafish (Danio rerio) embryos, Comp Biochem Physiol C Toxicol
727 Pharmacol, 193 (2017) 18-29.
728 [34] A. Eufrasio, C. Perrod, F.J. Ferreira, M. Duque, M. Galhardo, J. Bessa, In Vivo Reporter
729 Assays Uncover Changes in Enhancer Activity Caused by Type 2 Diabetes-Associated Single
730 Nucleotide Polymorphisms, Diabetes, 69 (2020) 2794-2805.
731 [35] N. Tiso, E. Moro, F. Argenton, Zebrafish pancreas development, Mol Cell Endocrinol,
732 312 (2009) 24-30.
733 [36] R. Li, Y. Shen, An old method facing a new challenge: re-visiting housekeeping proteins
734 as internal reference control for neuroscience research, Life Sci, 92 (2013) 747-751.
735 [37] J. Jumper, R. Evans, A. Pritzel, T. Green, M. Figurnov, O. Ronneberger, K.
736 Tunyasuvunakool, R. Bates, A. Zidek, A. Potapenko, A. Bridgland, C. Meyer, S.A.A. Kohl,
737 A.J. Ballard, A. Cowie, B. Romera-Paredes, S. Nikolov, R. Jain, J. Adler, T. Back, S. Petersen,
738 D. Reiman, E. Clancy, M. Zielinski, M. Steinegger, M. Pacholska, T. Berghammer, S.
739 Bodenstein, D. Silver, O. Vinyals, A.W. Senior, K. Kavukcuoglu, P. Kohli, D. Hassabis,
740 Highly accurate protein structure prediction with AlphaFold, Nature, 596 (2021) 583-589.
741 [38] M. Varadi, S. Anyango, M. Deshpande, S. Nair, C. Natassia, G. Yordanova, D. Yuan, O.
742 Stroe, G. Wood, A. Laydon, A. Zidek, T. Green, K. Tunyasuvunakool, S. Petersen, J. Jumper,
743 E. Clancy, R. Green, A. Vora, M. Lutfi, M. Figurnov, A. Cowie, N. Hobbs, P. Kohli, G.
744 Kleywegt, E. Birney, D. Hassabis, S. Velankar, AlphaFold Protein Structure Database:
745 massively expanding the structural coverage of protein-sequence space with high-accuracy
746 models, Nucleic Acids Res, 50 (2022) D439-D444.
747 [39] E.F. Pettersen, T.D. Goddard, C.C. Huang, E.C. Meng, G.S. Couch, T.I. Croll, J.H. Morris,
748 T.E. Ferrin, UCSF ChimeraX: Structure visualization for researchers, educators, and
749 developers, Protein Sci, 30 (2021) 70-82.

750 [40] J.M. Axten, J.R. Medina, Y. Feng, A. Shu, S.P. Romeril, S.W. Grant, W.H. Li, D.A.
751 Heerding, E. Minthorn, T. Mencken, C. Atkins, Q. Liu, S. Rabindran, R. Kumar, X. Hong, A.
752 Goetz, T. Stanley, J.D. Taylor, S.D. Sigethy, G.H. Tomberlin, A.M. Hassell, K.M. Kahler,
753 L.M. Shewchuk, R.T. Gampe, Discovery of 7-methyl-5-(1-{[3-
754 (trifluoromethyl)phenyl]acetyl}-2,3-dihydro-1H-indol-5-yl)-7H-p yrrolo[2,3-d]pyrimidin-4-
755 amine (GSK2606414), a potent and selective first-in-class inhibitor of protein kinase R (PKR)-
756 like endoplasmic reticulum kinase (PERK), J Med Chem, 55 (2012) 7193-7207.
757 [41] C. Chintha, A. Carlesso, A.M. Gorman, A. Samali, L.A. Eriksson, Molecular modeling
758 provides a structural basis for PERK inhibitor selectivity towards RIPK1, RSC Adv, 10 (2019)
759 367-375.
760 [42] O. Carugo, S. Pongor, A normalized root-mean-square distance for comparing protein
761 three-dimensional structures, Protein Sci, 10 (2001) 1470-1473.
762 [43] M.M. Rahman, T. Basta, J. Teng, M. Lee, B.T. Worrell, M.H.B. Stowell, R.E. Hibbs,
763 Structural mechanism of muscle nicotinic receptor desensitization and block by curare, Nat
764 Struct Mol Biol, 29 (2022) 386-394.
765 [44] L. Guzman, G. Besa, D. Linares, L. González, C. Pont, M. Bartolini, A. Haigis, J. Legradi,
766 D. Muñoz-Torrero, J. Gómez-Catalán, M. Barenys, Evaluation of the effects of
767 acetylcholinesterase inhibitors in the zebrafish touch-evoked response: quantitative vs.
768 qualitative assessment, Environ Sci Eur, 32 (2020) 12.
769 [45] A. Sumegi, Z. Hendrik, T. Gall, E. Felszeghy, K. Szakszon, P. Antal-Szalmas, L. Beke,
770 A. Papp, G. Mehes, J. Balla, G. Balla, A novel splice site indel alteration in the EIF2AK3 gene
771 is responsible for the first cases of Wolcott-Rallison syndrome in Hungary, BMC Med Genet,
772 21 (2020) 61.
773 [46] O. Rubio-Cabezas, A.M. Patch, J.A. Minton, S.E. Flanagan, E.L. Edghill, K. Hussain, A.
774 Balafrej, A. Deeb, C.R. Buchanan, I.G. Jefferson, A. Mutair, G. Neonatal Diabetes

775 International Collaborative, A.T. Hattersley, S. Ellard, Wolcott-Rallison syndrome is the most
776 common genetic cause of permanent neonatal diabetes in consanguineous families, J Clin
777 Endocrinol Metab, 94 (2009) 4162-4170.
778 [47] K. Iida, Y. Li, B.C. McGrath, A. Frank, D.R. Cavener, PERK eIF2 alpha kinase is required
779 to regulate the viability of the exocrine pancreas in mice, BMC Cell Biol, 8 (2007) 38.
780 [48] D. Aldrian, C. Bochdansky, A.M. Kavallar, C. Mayerhofer, A. Deeb, A. Habeb, A.
781 Romera Rabasa, A. Khadilkar, A. Ucar, B. Knoppke, D. Zafeiriou, M. Lang-Muritano, M.
782 Miqdady, S. Judmaier, V. McLin, V. Furdela, T. Muller, G.F. Vogel, Natural history of
783 Wolcott-Rallison syndrome: A systematic review and follow-up study, Liver Int, 44 (2024)
784 811-822.
785 [49] F. Zindler, F. Beedgen, D. Brandt, M. Steiner, D. Stengel, L. Baumann, T. Braunbeck,
786 Analysis of tail coiling activity of zebrafish (Danio rerio) embryos allows for the differentiation
787 of neurotoxicants with different modes of action, Ecotoxicol Environ Saf, 186 (2019) 109754.
788 [50] A.C. Roberts, J. Chornak, J.B. Alzagatiti, D.T. Ly, B.R. Bill, J. Trinkeller, K.C. Pearce,
789 R.C. Choe, C.S. Campbell, D. Wong, E. Deutsch, S. Hernandez, D.L. Glanzman, Rapid
790 habituation of a touch-induced escape response in Zebrafish (Danio rerio) Larvae, PLoS One,
791 14 (2019) e0214374.
792 [51] M. von Wyl, S. Konemann, C. Vom Berg, Different developmental insecticide exposure
793 windows trigger distinct locomotor phenotypes in the early life stages of zebrafish,
794 Chemosphere, 317 (2023) 137874.
795 [52] J. Berger, T. Sztal, P.D. Currie, Quantification of birefringence readily measures the level
796 of muscle damage in zebrafish, Biochem Biophys Res Commun, 423 (2012) 785-788.
797 [53] C.M. Thornton, D.J. Carson, F.J. Stewart, Autopsy findings in the Wolcott-Rallison
798 syndrome, Pediatr Pathol Lab Med, 17 (1997) 487-496.

799 [54] J.A. Moreno, M. Halliday, C. Molloy, H. Radford, N. Verity, J.M. Axten, C.A. Ortori,
800 A.E. Willis, P.M. Fischer, D.A. Barrett, G.R. Mallucci, Oral treatment targeting the unfolded
801 protein response prevents neurodegeneration and clinical disease in prion-infected mice, Sci
802 Transl Med, 5 (2013) 206ra138.
803 [55] R. Cagnetta, H.H. Wong, C.K. Frese, G.R. Mallucci, J. Krijgsveld, C.E. Holt,
804 Noncanonical Modulation of the eIF2 Pathway Controls an Increase in Local Translation
805 during Neural Wiring, Mol Cell, 73 (2019) 474-489 e475.
806 [56] D. Rojas-Rivera, T. Delvaeye, R. Roelandt, W. Nerinckx, K. Augustyns, P. Vandenabeele,
807 M.J.M. Bertrand, When PERK inhibitors turn out to be new potent RIPK1 inhibitors: critical
808 issues on the specificity and use of GSK2606414 and GSK2656157, Cell Death Differ, 24
809 (2017) 1100-1110.
810 [57] M. Mahameed, T. Wilhelm, O. Darawshi, A. Obiedat, W.S. Tommy, C. Chintha, T.
811 Schubert, A. Samali, E. Chevet, L.A. Eriksson, M. Huber, B. Tirosh, The unfolded protein
812 response modulators GSK2606414 and KIRA6 are potent KIT inhibitors, Cell Death Dis, 10
813 (2019) 300.
814 [58] W. Wen, J. Chen, Y. Zhou, G. Li, Y. Zhang, Loss of Ripk3 attenuated neutrophil
815 accumulation in a lipopolysaccharide-induced zebrafish inflammatory model, Cell Death
816 Discov, 8 (2022) 88.
817 [59] K.A. Hultman, N. Bahary, L.I. Zon, S.L. Johnson, Gene Duplication of the zebrafish kit
818 ligand and partitioning of melanocyte development functions to kit ligand a, PLoS Genet, 3
819 (2007) e17.
820 [60] D.J.M. Bergen, E. Kague, C.L. Hammond, Zebrafish as an Emerging Model for
821 Osteoporosis: A Primary Testing Platform for Screening New Osteo-Active Compounds, Front
822 Endocrinol (Lausanne), 10 (2019) 6.

823 [61] Y. Li, K. Iida, J. O'Neil, P. Zhang, S. Li, A. Frank, A. Gabai, F. Zambito, S.H. Liang, C.J.
824 Rosen, D.R. Cavener, PERK eIF2alpha kinase regulates neonatal growth by controlling the
825 expression of circulating insulin-like growth factor-I derived from the liver, Endocrinology,
826 144 (2003) 3505-3513.
827 [62] D. Feng, J. Wei, S. Gupta, B.C. McGrath, D.R. Cavener, Acute ablation of PERK results
828 in ER dysfunctions followed by reduced insulin secretion and cell proliferation, BMC Cell
829 Biol, 10 (2009) 61.
830 [63] W. Zhang, D. Feng, Y. Li, K. Iida, B. McGrath, D.R. Cavener, PERK EIF2AK3 control
831 of pancreatic beta cell differentiation and proliferation is required for postnatal glucose
832 homeostasis, Cell Metab, 4 (2006) 491-497.
833 [64] C.R. Sowers, R. Wang, R.A. Bourne, B.C. McGrath, J. Hu, S.C. Bevilacqua, J.C. Paton,
834 A.W. Paton, S. Collardeau-Frachon, M. Nicolino, D.R. Cavener, The protein kinase
835 PERK/EIF2AK3 regulates proinsulin processing not via protein synthesis but by controlling
836 endoplasmic reticulum chaperones, J Biol Chem, 293 (2018) 5134-5149.
837 [65] A. Welters, T. Meissner, K. Konrad, C. Freiberg, K. Warncke, S. Judmaier, O.
838 Kordonouri, M. Wurm, M. Papsch, G. Fitzke, S.C. Schmidt, S.R. Tittel, R.W. Holl, Diabetes
839 management in Wolcott-Rallison syndrome: analysis from the German/Austrian DPV
840 database, Orphanet J Rare Dis, 15 (2020) 100.
841 [66] J.B. Moss, P. Koustubhan, M. Greenman, M.J. Parsons, I. Walter, L.G. Moss,
842 Regeneration of the pancreas in adult zebrafish, Diabetes, 58 (2009) 1844-1851.
843 [67] H. Pisharath, J.M. Rhee, M.A. Swanson, S.D. Leach, M.J. Parsons, Targeted ablation of
844 beta cells in the embryonic zebrafish pancreas using E. coli nitroreductase, Mech Dev, 124
845 (2007) 218-229.

[68] S.N. Asl, R. Vakili, S. Vakili, F. Soheilipour, M. Hashemipour, S. Ghahramani, E. De Franco, H. Yaghootkar, Wolcott-Rallison syndrome in Iran: a common cause of neonatal diabetes, J Pediatr Endocrinol Metab, 32 (2019) 607-613.

[69] F. Longo, M. Mancini, P.L. Ibraheem, S. Aryal, C. Mesini, J.C. Patel, E. Penhos, N. Rahman, M. Mamcarz, E. Santini, M.E. Rice, E. Klann, Cell-type-specific disruption of PERK-eIF2alpha signaling in dopaminergic neurons alters motor and cognitive function, Mol Psychiatry, 26 (2021) 6427-6450.

[70] R. Bejiqi, R. Retkoceri, N. Zeka, R. Bejiqi, S. Bejic, An Infant With Neonatal Diabetes and Double Outlet Right Ventricle - Wolcott- Rallison syndrome, Med Arch, 72 (2018) 289-291.

[71] D. Bournele, D. Beis, Zebrafish models of cardiovascular disease, Heart Fail Rev, 21 (2016) 803-813.

[72] C. Cornet, V. Di Donato, J. Terriente, Combining Zebrafish and CRISPR/Cas9: Toward a More Efficient Drug Discovery Pipeline, Front Pharmacol, 9 (2018) 703.

A Global amino acid comparison

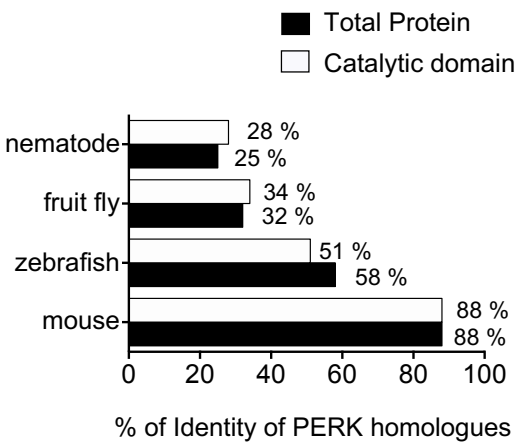

B Comparison of vital* amino acids in catalytic domain

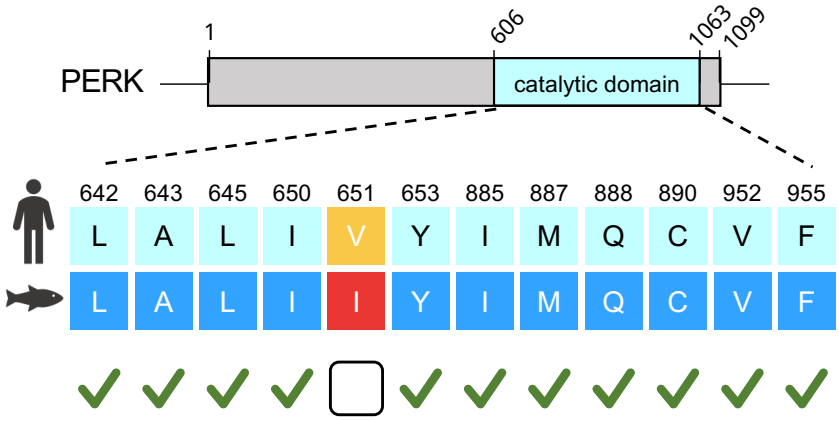

* 12 vital amino acids for GSK2606414 binding

valine (V) and isoleucine (I) are both hydrophobic

C Molecular visualization of GSK binding to PERK

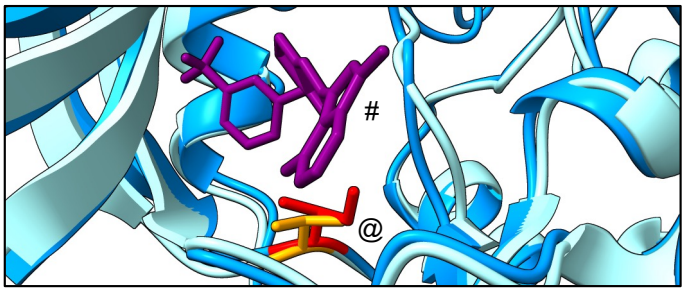

human PERK

zebrafish PERK

@, valine 651 (human)

@, isoleucine (zebrafish)

#, GSK2606414 (GSK)

D Structural similarity of human vs. zebrafish PERK

Root Mean Square Deviation		
Total protein	0.868 Å	**High similarity** (0-1 Å)
Catalytic domain	0.371 Å	**High similarity** (0-1 Å)

Figure 1

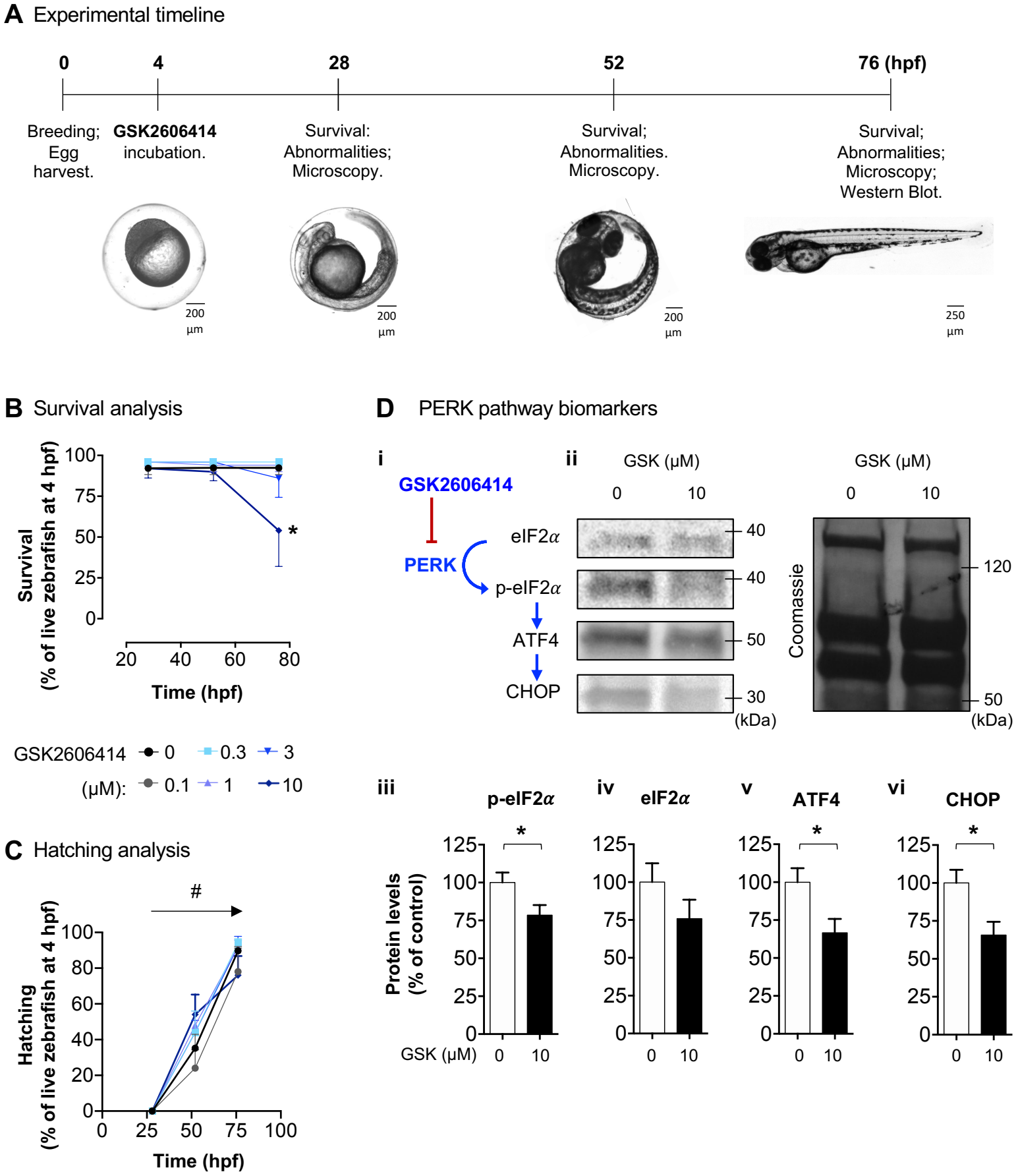
A Experimental timeline
0
4
28
52
76 (hpf)
Breeding; Egg harvest.
GSK2606414 incubation.
Survival: Abnormalities; Microscopy.
Survival; Abnormalities. Microscopy.
Survival; Abnormalities; Microscopy; Western Blot.
200 µm
200 µm
200 µm
250 µm
B Survival analysis
Survival (% of live zebrafish at 4 hpf)
Time (hpf)
GSK2606414 (µM): 0 0.3 3 0.1 1 10
C Hatching analysis
Hatching (% of live zebrafish at 4 hpf)
Time (hpf)
D PERK pathway biomarkers
i
GSK2606414
PERK
eIF2α
p-eIF2α
ATF4
CHOP
ii
GSK (µM)
0 10
40
40
50
30
(kDa)
Coomassie
120
50
(kDa)
iii p-eIF2α
iv eIF2α
v ATF4
vi CHOP
Protein levels (% of control)
GSK (µM) 0 10

Figure 2

A Morphological defects

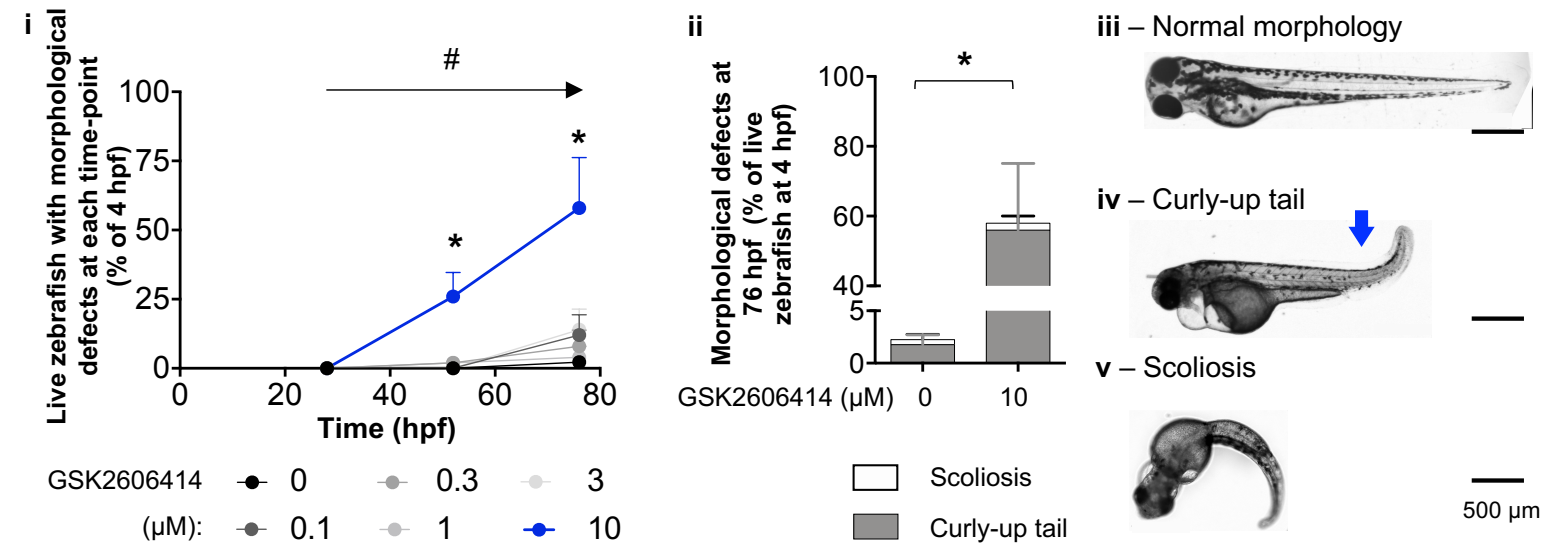

B Trunk-tail angle

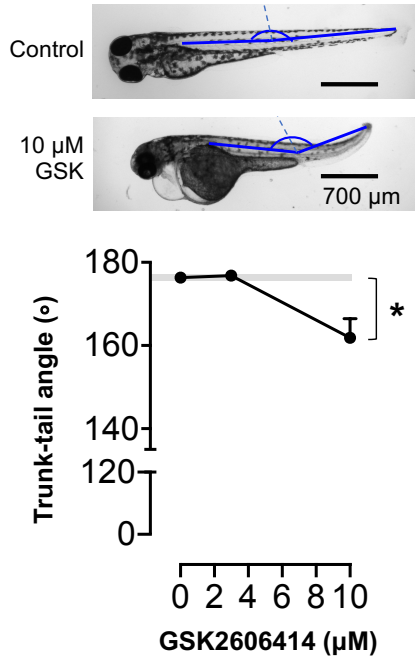

C Body length

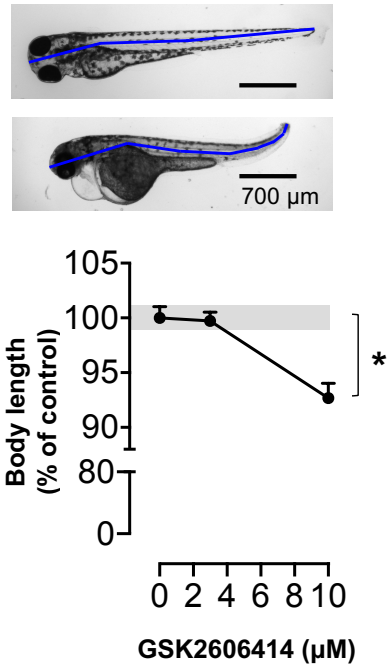

D Positive control for tubocurarine (dTC)

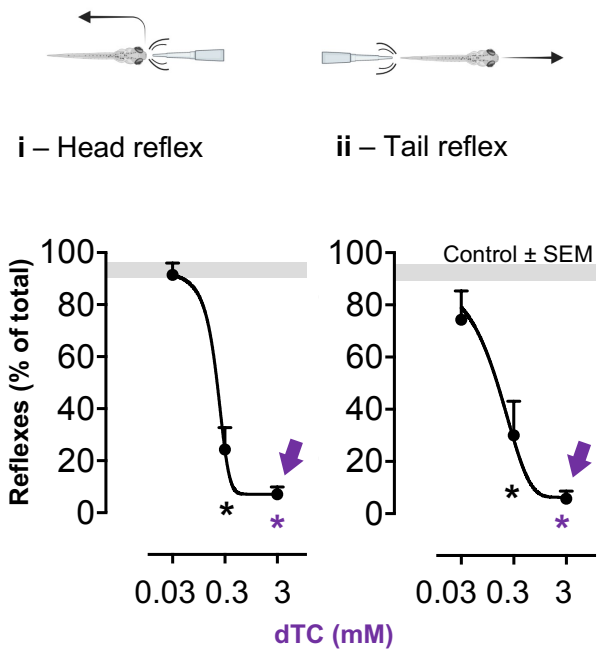

E The muscle relaxant tubocurarine (dTC) does not rescue the curly-up tail evoked by GSK2606414

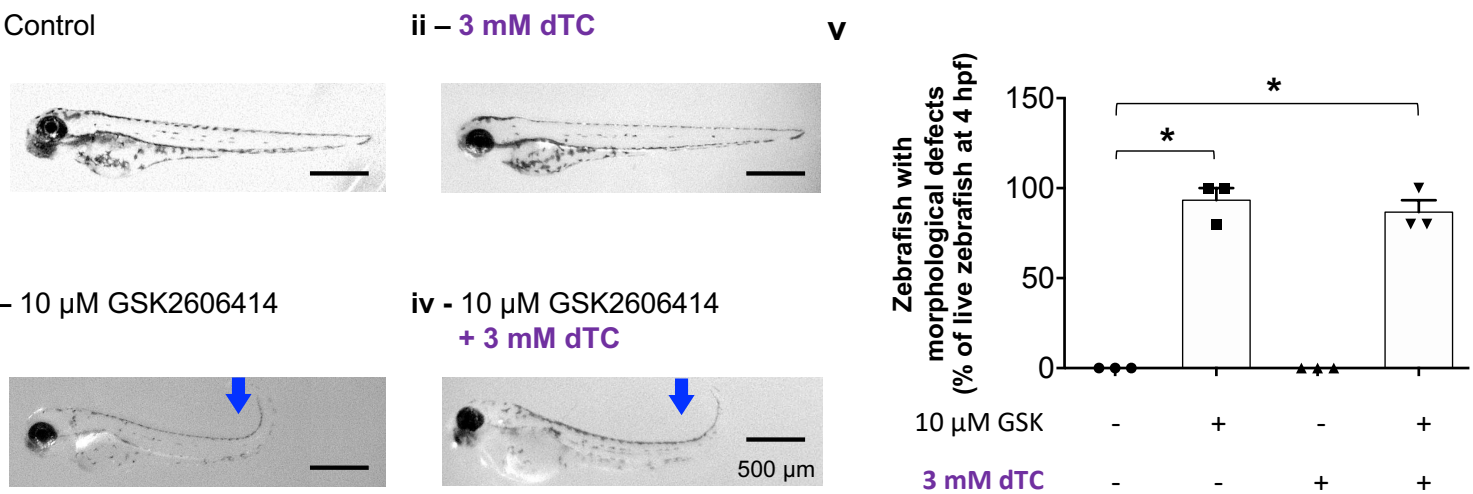

Figure 3

Figure 4

A Pancreatic development

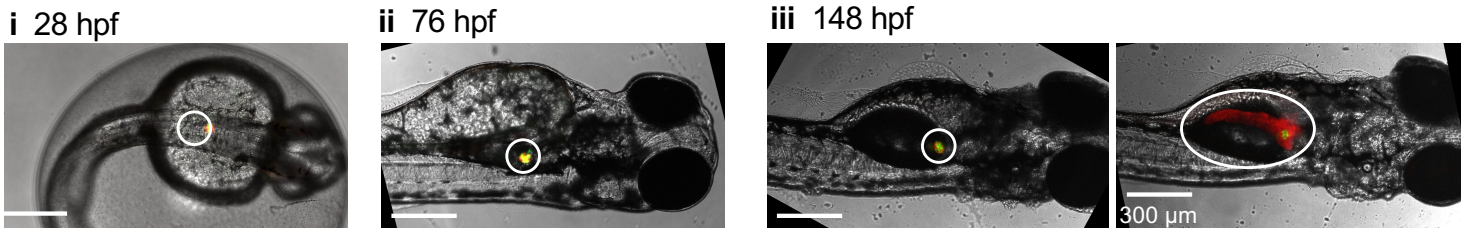

B

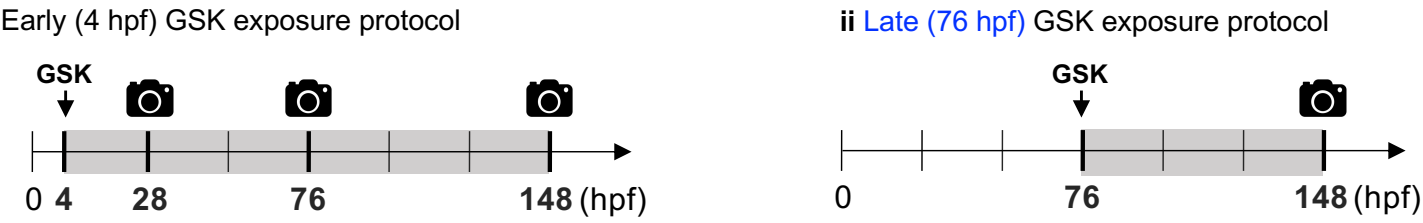

C *ins:GFP* (*β* cell; endocrine)

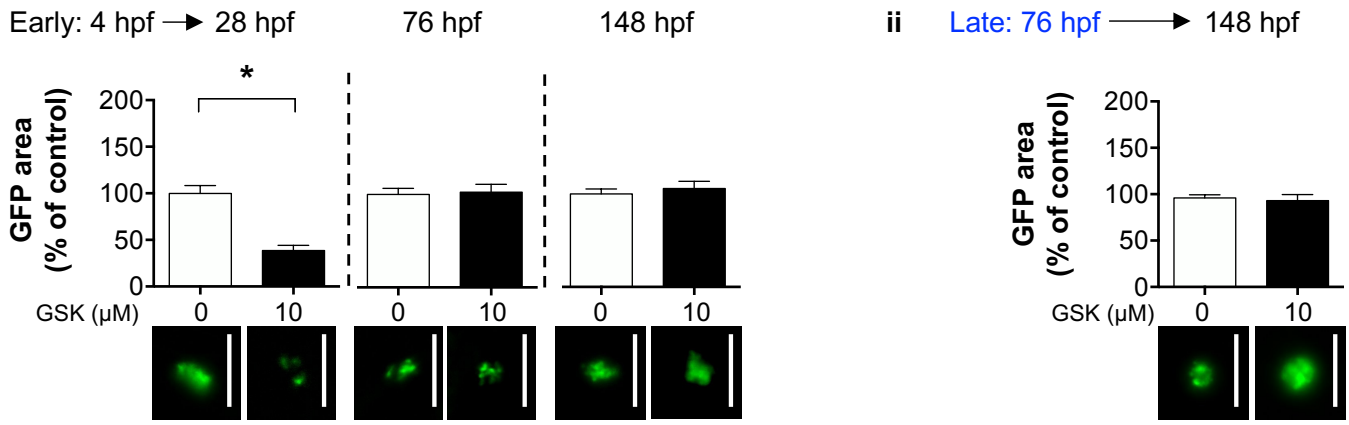

D *sst:mCherry* (*δ* cell; endocrine)

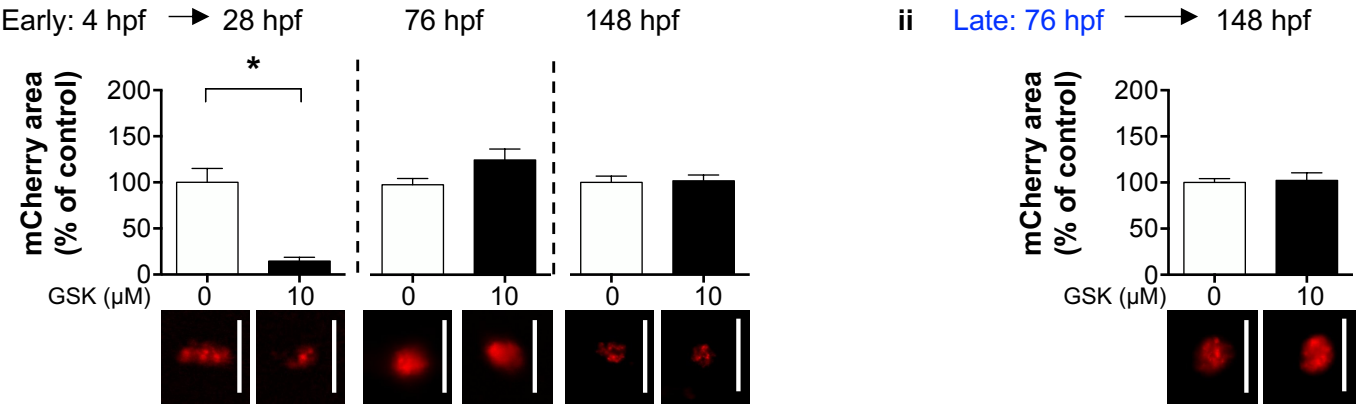

E *ela:mCherry* (exocrine)

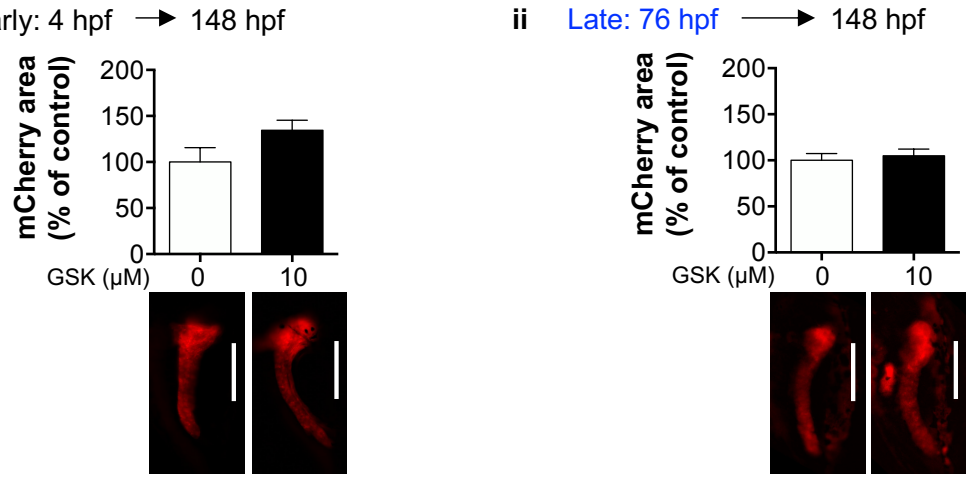

A 2-NBD glucose uptake to neuromasts

i Control

ii 10 μM GSK2606414

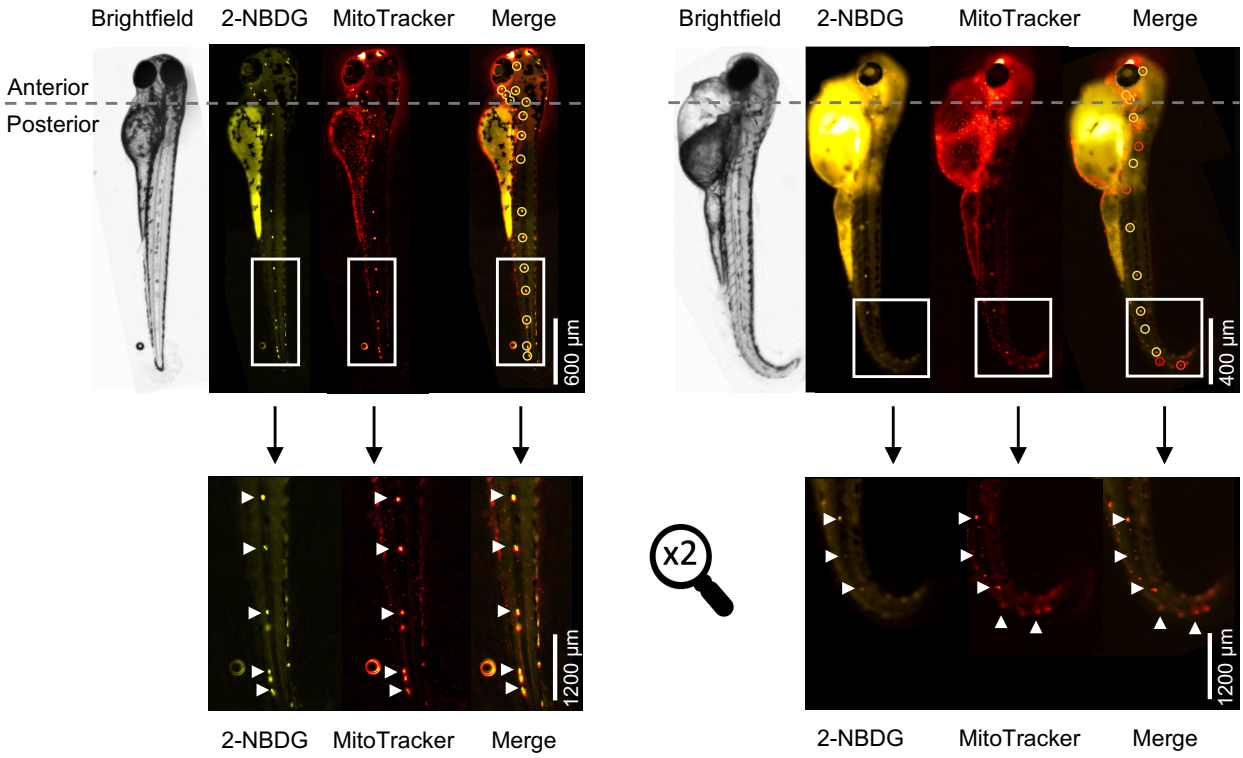

B Neuromast quantification

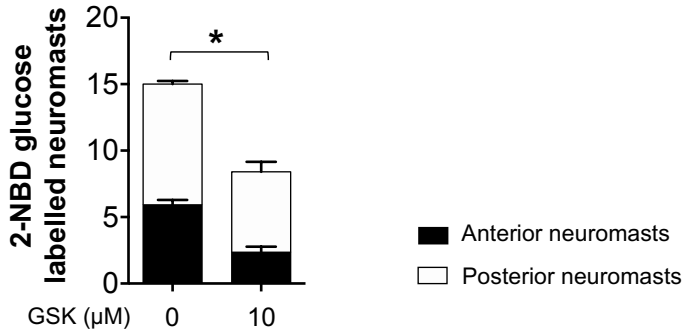

Figure 5

A Tail coiling events (28 hpf)

i

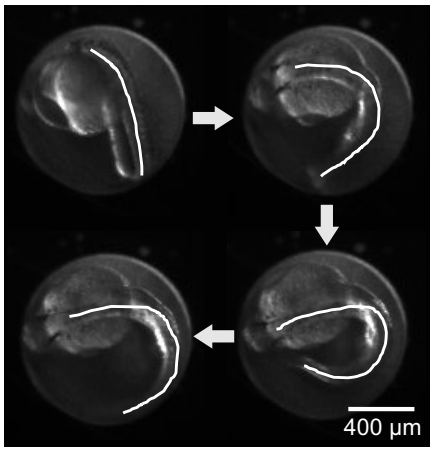

ii

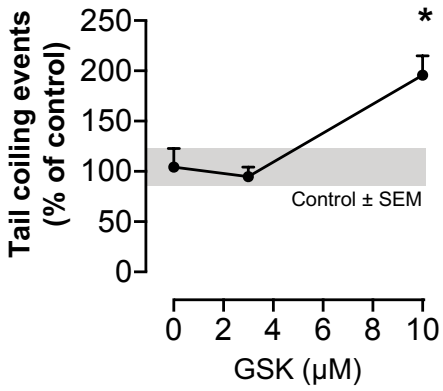

B Touch-evoked escape responses (76 hpf)

i

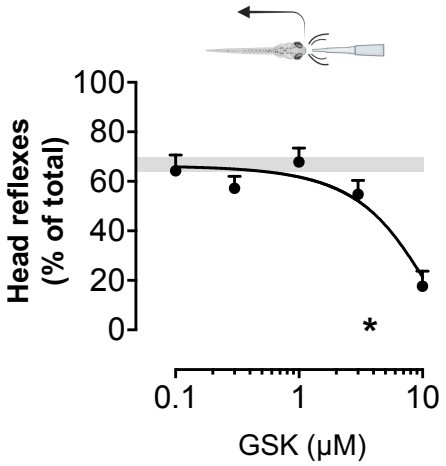

ii

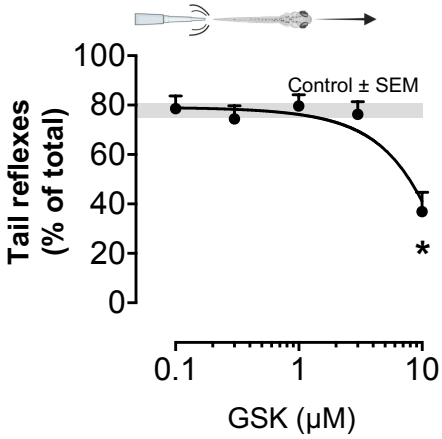

C Birefringence assay (76 hpf)

i

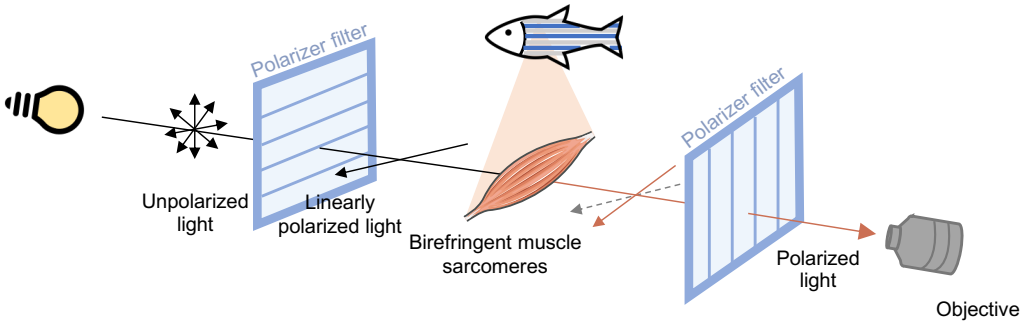

ii

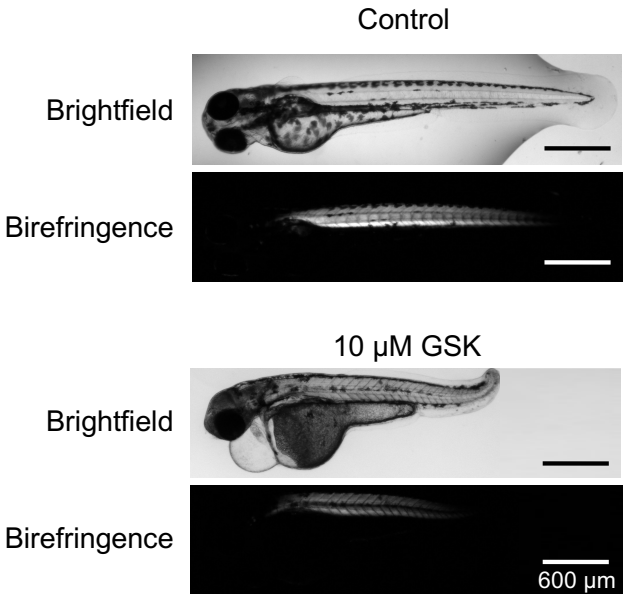

iii

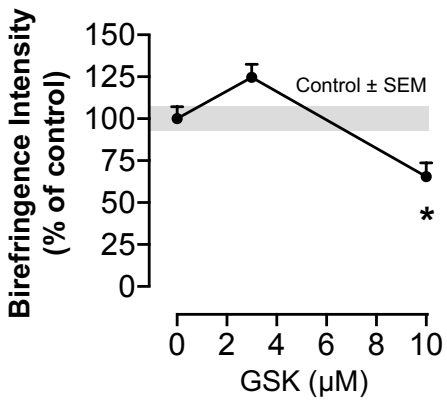

Figure 6

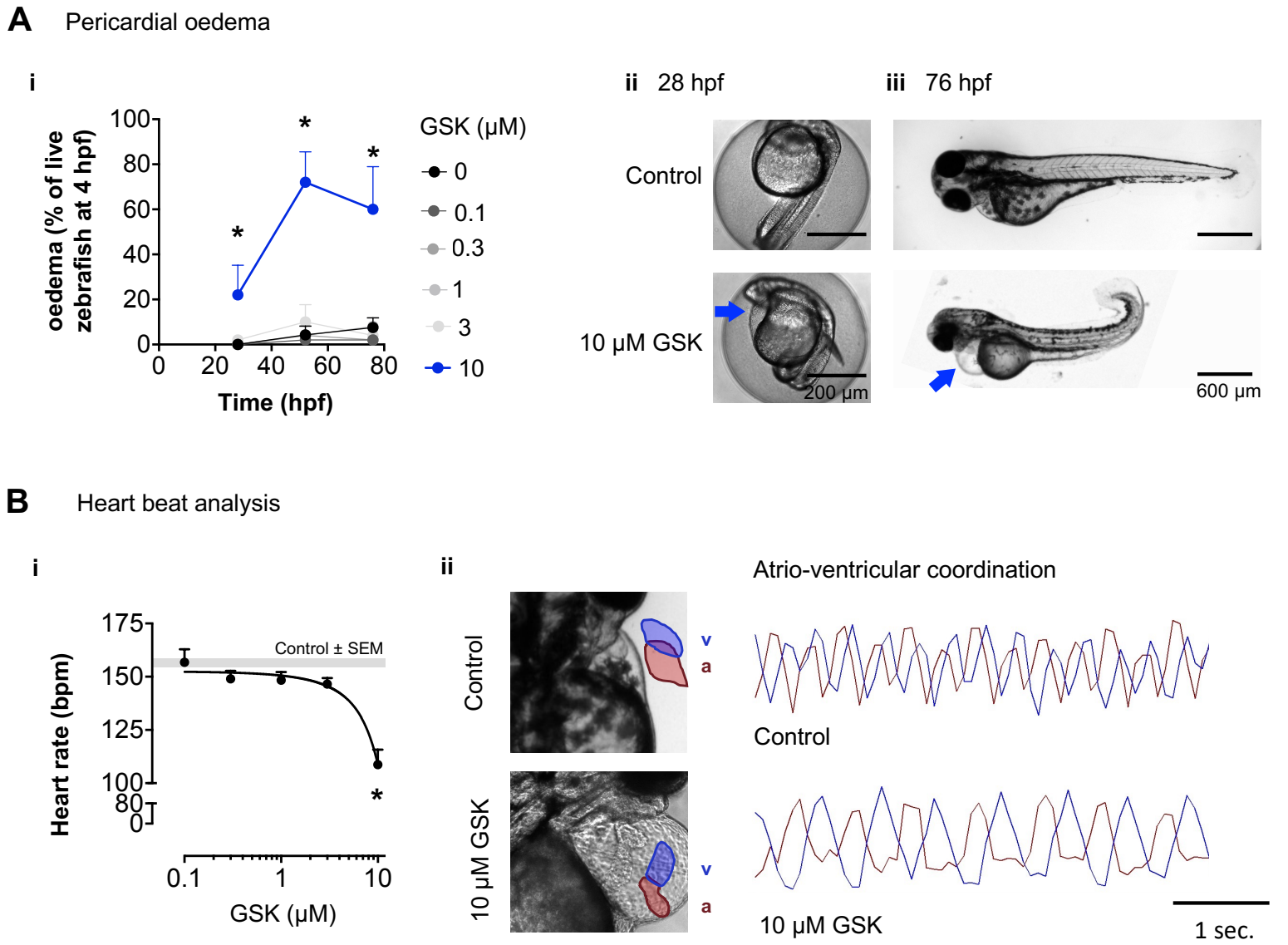
A
Pericardial oedema
i
oedema (% of live zebrafish at 4 hpf)
100
80
60
40
20
0
0
20
40
60
80
Time (hpf)
*
*
*
GSK (μM)
0
0.1
0.3
1
3
10
ii 28 hpf
iii 76 hpf
Control
10 μM GSK
200 μm
600 μm
B
Heart beat analysis
i
Heart rate (bpm)
175
150
125
100
80
0
Control ± SEM
*
0.1
1
10
GSK (μM)
ii
Control
10 μM GSK
v
a
v
a
Atrio-ventricular coordination
Control
10 μM GSK
1 sec.

Figure 7

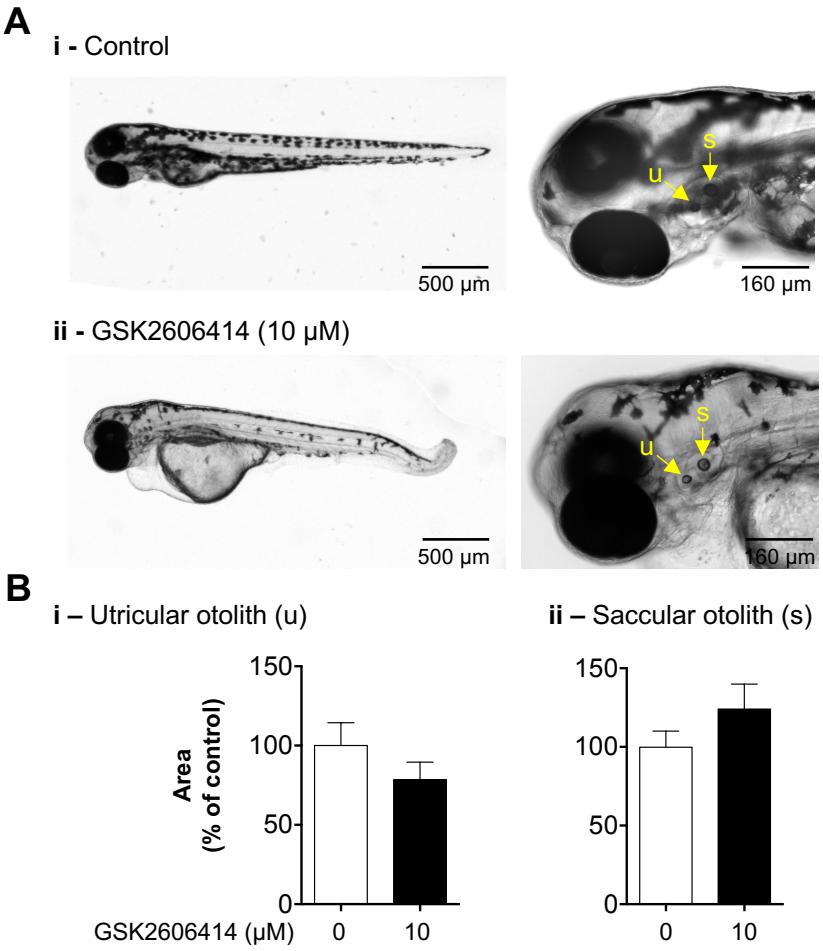

Supplementary Figure 1. GSK2606414 (GSK) does not alter zebrafish otolith area. **(A)** Representative images of zebrafish at 76hpf following treatment with control (0 µM GSK) or 10 µM GSK since 4 hpf. Arrows: (u) utricular/anterior otolith, (s) saccular/posterior otolith. **(B)** Mean ± SEM of the otolith area, $P > 0.05$, t-test, $n = 15$ larvae, 3 zebrafish experiments.

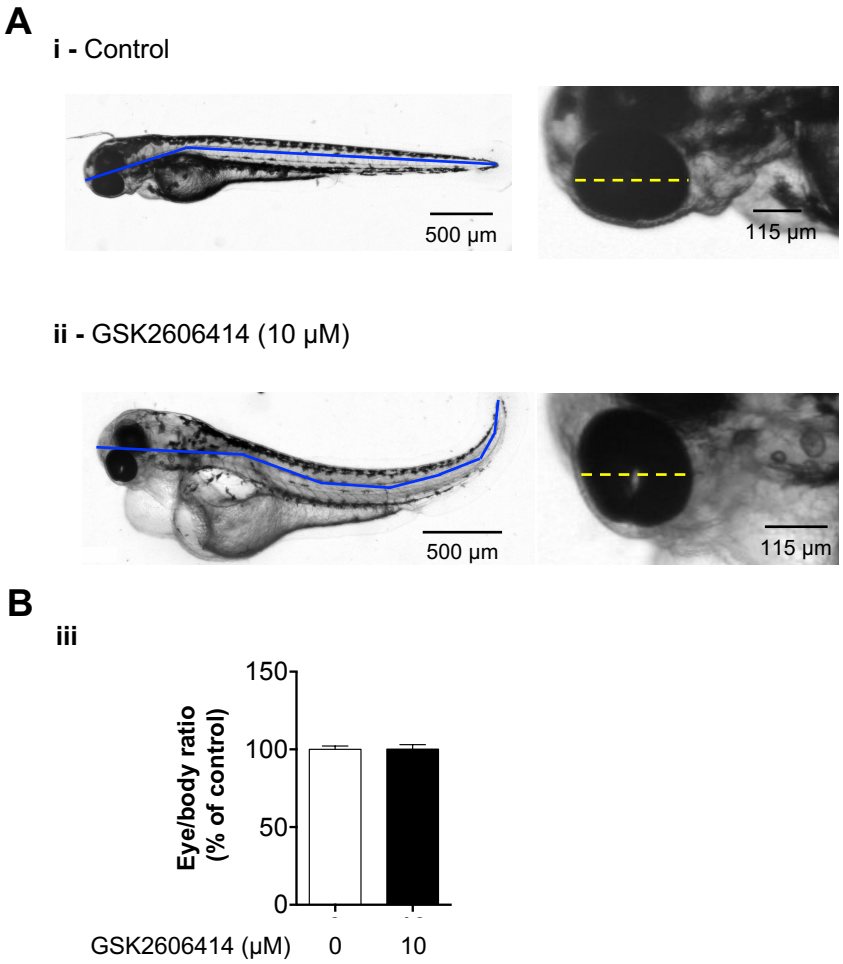

Supplementary Figure 2. GSK2606414 does not alter zebrafish eye/body ratio. **(A)** Representative images of zebrafish at 76hpf following treatment with control (0 µM GSK) or 10 µM GSK since 4 hpf. Solid blue lines: body length; dashed yellow lines: eye diameter. **(B)** Mean ± SEM of the eye/body ratio, $P > 0.05$, t-test, $n = 15$ zebrafish, 3 independent experiments.